Cell Reports

Article

CXCL4 drives fibrosis by promoting several key cellular and molecular processes

Graphical abstract

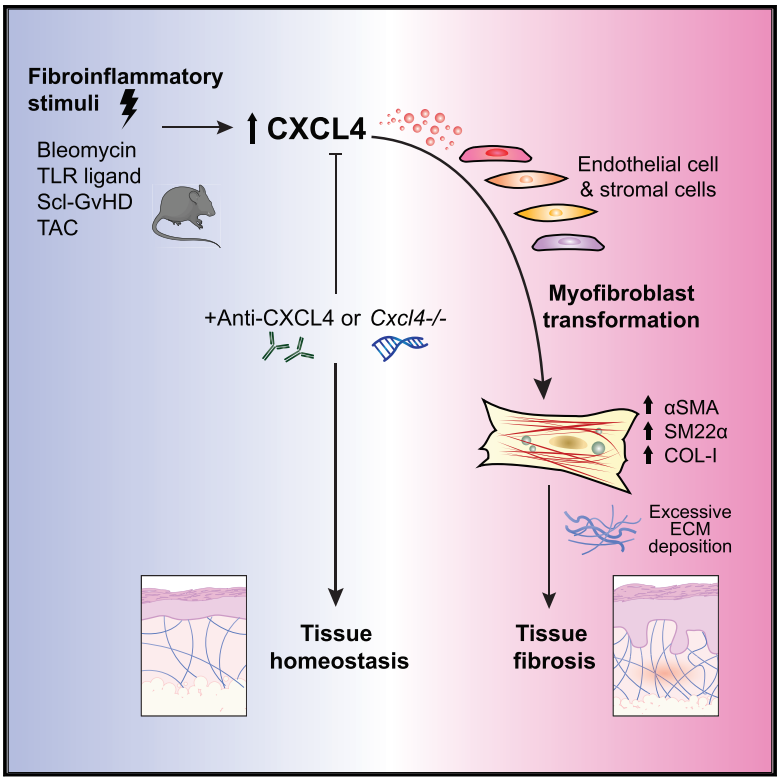

Highlights

- CXCL4 is increased in multiple fibrotic models resembling systemic sclerosis
- Absence of CXCL4 diminishes and overexpression aggravates bleomycin-induced fibrosis
- CXCL4 promotes myofibroblast transformation and collagen production
- CXCL4-induced endothelial-to-mesenchymal transition involves metabolic changes

Authors

Alsya J. Affandi, Tiago Carvalheiro, Andrea Ottria, ..., Joel A.G. van Roon, Timothy R.D.J. Radstake, Wioleta Marut

Correspondence

vmarut@gmail.com

In brief

Dysregulation of extracellular matrix homeostasis can lead to fibrotic disorders. Affandi et al. find that CXCL4 mediates fibrosis in multiple *in vivo* models by acting directly on endothelial cells and stromal cells, transforming them into myofibroblasts with excessive collagen production. Targeting CXCL4 suppresses fibrosis development, suggesting a potential therapeutic strategy.

Affandi et al., 2022, Cell Reports *38*, 110189
January 4, 2022
https://doi.org/10.1016/j.celrep.2021.110189

CellPress

Cell Reports

CellPress
OPEN ACCESS

Article

CXCL4 drives fibrosis by promoting several key cellular and molecular processes

Alsya J. Affandi,[1,2,3,4,12] Tiago Carvalheiro,[1,2,12] Andrea Ottria,[1,2] Judith J. de Haan,[5] Maike A.D. Brans,[5] Maarten M. Brandt,[6] Ralph G. Tieland,[1,2] Ana P. Lopes,[1,2] Beatriz Malvar Fernández,[1,2] Cornelis P.J. Bekker,[1,2] Maarten van der Linden,[1,2] Maili Zimmermann,[1,2] Barbara Giovannone,[1,7] Catharina G.K. Wichers,[1,2] Samuel Garcia,[1,2] Michael de Kok,[3] Giuseppina Stifano,[4] Yan Juan Xu,[8] M. Anna Kowalska,[9,10] Maaike Waasdorp,[3] Caroline Cheng,[8] Susan Gibbs,[3,11] Saskia C.A. de Jager,[5] Joel A.G. van Roon,[1,2] Timothy R.D.J. Radstake,[1,2] and Wioleta Marut[1,2,13,*]

[1]Center for Translational Immunology, University Medical Center Utrecht, Utrecht University, Utrecht, the Netherlands
[2]Department of Rheumatology and Clinical Immunology, University Medical Center Utrecht, Utrecht University, Utrecht, the Netherlands
[3]Department of Molecular Cell Biology and Immunology, Amsterdam University Medical Center, Vrije Universiteit Amsterdam, Amsterdam, the Netherlands
[4]Rheumatology Section, Boston University School of Medicine, Boston, MA, USA
[5]Department of Experimental Cardiology, University Medical Center Utrecht, Utrecht University, Utrecht, the Netherlands
[6]Experimental Cardiology, Department of Cardiology, Thoraxcenter, Erasmus University Medical Center, Rotterdam, the Netherlands
[7]Department of Dermatology, University Medical Center Utrecht, Utrecht University, Utrecht, the Netherlands
[8]Department of Nephrology and Hypertension, University Medical Center Utrecht, Utrecht University, Utrecht, the Netherlands
[9]Department of Hematology, Children's Hospital of Philadelphia, Philadelphia, PA, USA
[10]Institute of Medical Biology, Polish Academy of Science, Lodz, Poland
[11]Department of Oral Cell Biology, Academic Centre for Dentistry (ACTA), University of Amsterdam and Vrije Universiteit Amsterdam, Amsterdam, the Netherlands
[12]These authors contributed equally
[13]Lead contact
*Correspondence: vmarut@gmail.com
https://doi.org/10.1016/j.celrep.2021.110189

SUMMARY

Fibrosis is a major cause of mortality worldwide, characterized by myofibroblast activation and excessive extracellular matrix deposition. Systemic sclerosis is a prototypic fibrotic disease in which CXCL4 is increased and strongly correlates with skin and lung fibrosis. Here we aim to elucidate the role of CXCL4 in fibrosis development. CXCL4 levels are increased in multiple inflammatory and fibrotic mouse models, and, using CXCL4-deficient mice, we demonstrate the essential role of CXCL4 in promoting fibrotic events in the skin, lungs, and heart. Overexpressing human CXCL4 in mice aggravates, whereas blocking CXCL4 reduces, bleomycin-induced fibrosis. Single-cell ligand-receptor analysis predicts CXCL4 to affect endothelial cells and fibroblasts. *In vitro*, we confirm that CXCL4 directly induces myofibroblast differentiation and collagen synthesis in different precursor cells, including endothelial cells, by stimulating endothelial-to-mesenchymal transition. Our findings identify a pivotal role of CXCL4 in fibrosis, further substantiating the potential role of neutralizing CXCL4 as a therapeutic strategy.

INTRODUCTION

In fibrotic disorders, an excessive deposition of extracellular matrix (ECM) leads to obliteration of the original tissue architecture and function (Rockey et al., 2015). During this process, many ECM components are produced by activated myofibroblasts, characterized by *de novo* α-smooth muscle actin (α-SMA) expression (Hinz et al., 2007). Although myofibroblasts are required for physiological tissue repair mechanisms such as wound healing, their persistence can lead to development of fibrosis. The origin of these cells was initially assumed to be tissue-resident fibroblasts, but other cell types can also give rise to formation of myofibroblasts (myofibroblast transformation [MT]). For instance, conversion of cells of endothelial origin (endothelial MT [EndMT]) or epithelial origin (epithelial MT [EMT]) to mesenchymal-like cells is likely to play an essential role in systemic sclerosis (SSc) and other chronic fibrotic disorders (Hinz et al., 2007; Mack and Yanagita, 2015). The transformation of myofibroblasts from precursor cells is thought to be driven mainly by transforming growth factor β (TGF-β), but other fibrogenic cytokines derived from immune cells can also contribute to this process (Kendall and Feghali-Bostwick, 2014; Lafyatis, 2014).

SSc is a prototypical fibrotic disease characterized by fibrosis in the skin and multiple internal organs and is often preceded by chronic inflammation and vascular alterations (Ho et al., 2014; Varga and Abraham, 2007). With the purpose of delineating the underlying causes of the disease, we previously found the chemokine CXCL4 to be increased in the circulation

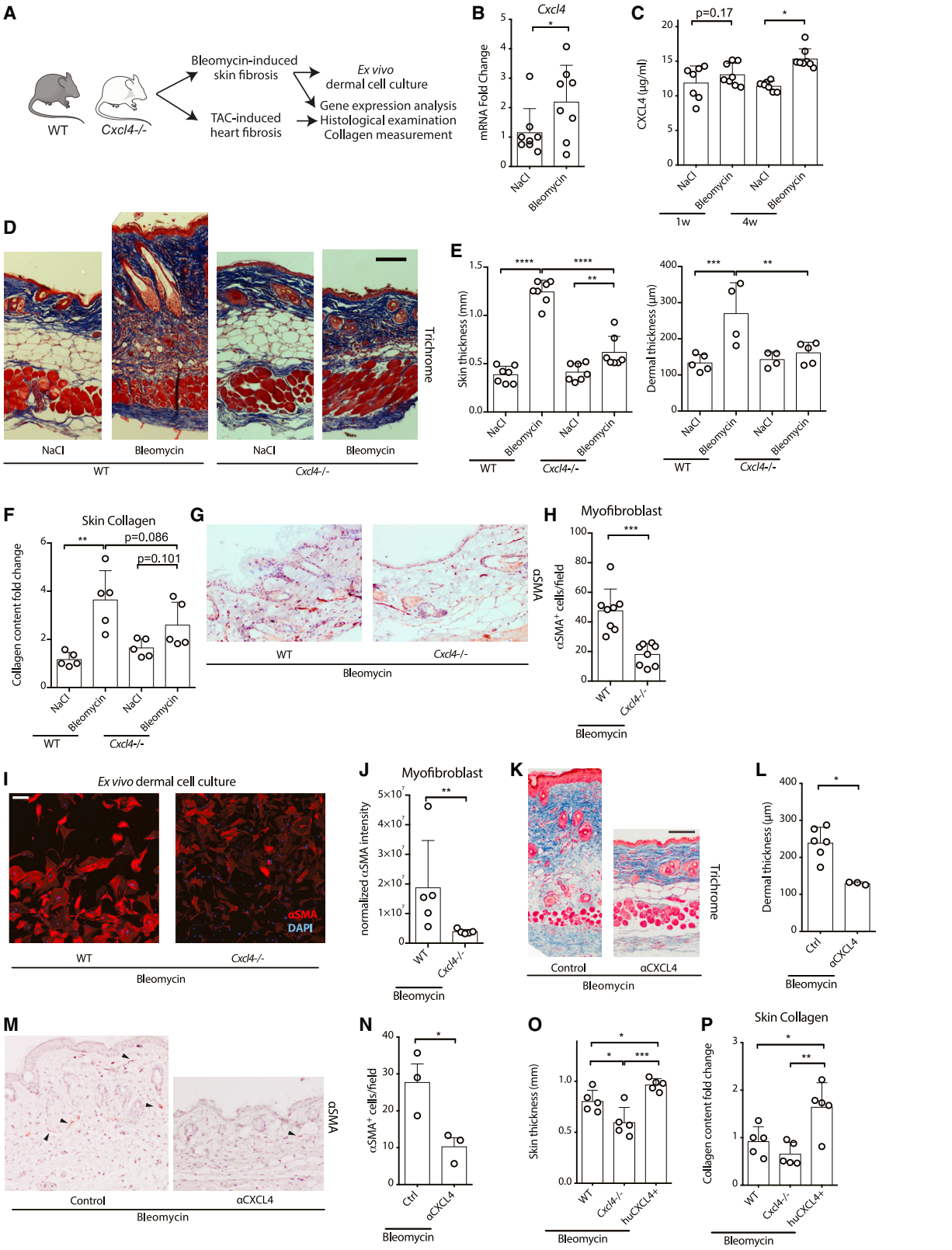

(legend on next page)

and skin of individuals with SSc, predicting the progression of skin and lung fibrosis (van Bon et al., 2014a). CXCL4 is a multifunctional chemokine that can target virtually all cells in the vasculature, and it is involved in numerous biological processes, including modulation of immune responses and angiogenesis (van Bon et al., 2014a; Duan et al., 2008; Van Raemdonck et al., 2015). CXCL4 has a pro-inflammatory role for multiple cells, including promoting production of interleukin-6 (IL-6) and tumor necrosis factor alpha (TNF-α) in monocytes (Kasper et al., 2010; Scheuerer et al., 2000), priming Toll-like receptor (TLR) responses of monocyte-derived dendritic cells (Silva-Cardoso et al., 2017), as well as boosting IL-17 production in CD4 T cells (Affandi et al., 2018). CXCL4 has been shown to be increased in inflammatory diseases, including inflammatory bowel disease, psoriasis, atherosclerosis, and rheumatoid arthritis (Van Raemdonck et al., 2015; Tamagawa-Mineoka et al., 2008; Yeo et al., 2016), as well as fibrotic disorders, such as chronic liver fibrosis, cystic fibrosis, and myelofibrosis (Burstein et al., 1984; Schwarz et al., 2003; Zaldivar et al., 2010). Its importance in disease pathogenesis has been shown in animal studies, where CXCL4-deficient mice were protected from disease development in atherosclerosis, acute lung injury, and liver fibrosis models (Grommes et al., 2012; Koenen et al., 2009; Zaldivar et al., 2010). Furthermore, CXCL4 can directly suppress proliferation of endothelial cells and their expression of the transcription factor FLI1, a negative regulator of collagen synthesis (van Bon et al., 2014a). Although this series of observations is suggestive of the potential pro-fibrotic properties of CXCL4, it is currently unclear whether CXCL4 could play a direct role in initiating fibrotic processes via myofibroblast precursor cells, which is a crucial void in information given the lack of effective therapies for fibrosis.

Here we demonstrate increased levels of CXCL4 in multiple experimental models of inflammation and fibrosis and show proof of concept for CXCL4 as a therapeutic target, as genetic knockdown of CXCL4 in mice remarkably reduces fibrosis in the skin, lungs, and heart. Importantly, we show that blocking CXCL4 abrogates skin fibrosis, whereas overexpression of CXCL4 aggravates disease. In addition, we reveal a direct role of CXCL4 in formation of myofibroblasts from different human precursor cells *in vitro* and delineate the mechanisms involved. Our study establishes CXCL4 as a key component in fibrosis development and the potential of blocking CXCL4 as a promising therapeutic strategy.

RESULTS

CXCL4 is increased in inflammatory and fibrotic conditions

CXCL4 has been shown to be increased in SSc skin and a bleomycin-induced skin fibrosis model, the most widely accepted animal model for SSc (Ah Kioon et al., 2018). Upon subcutaneous bleomycin treatment for 7 days, *Cxcl4* (*Pf4*) mRNA expression was indeed increased in the skin of mice compared with saline controls (Figures 1A and 1B). Although changes in serum CXCL4 levels were only marginally higher after 7 days of treatment, CXCL4 levels were clearly increased after 28 days (Figure 1C). We further examined CXCL4 levels in other *in vivo* experimental models mimicking SSc or other forms of fibrosis. We performed chronic stimulation with the TLR ligands poly(I:C) and lipopolysaccharide (LPS), using a subcutaneously implanted mini-osmotic pump, to induce skin inflammation and fibrosis (Farina et al., 2010; Stifano et al., 2014) and observed increased expression of *Cxcl4* mRNA in the skin in both models (Figures S1A and S1B). Because CXCL4 has been implicated in other fibrotic diseases (Zaldivar et al., 2010), we utilized the scleroderma-like graft versus host disease model (Scl-GvHD) to induce skin fibrosis and the model of pressure overload-induced cardiac fibrosis by transverse aortic constriction (TAC) to further examine the notion that increased levels of CXCL4 are a generalized phenomenon in fibrosis. In line with this thought, CXCL4 levels were found to be increased in the serum and heart of the Scl-GvHD and TAC models, respectively (Figures S1C and S1D).

We and others have shown previously that CXCL4 accumulation in fibrotic skin is contributed mainly by plasmacytoid dendritic cells (Ah Kioon et al., 2018; van Bon et al., 2014a), whereas in atherosclerotic plaque and rheumatoid arthritis synovium, macrophages have been shown to be the major source of

Figure 1. CXCL4 is a critical factor required for bleomycin-induced skin and lung fibrosis

(A) Wild-type (WT) C57BL/6 or *Cxcl4*$^{-/-}$ mice were injected subcutaneously with bleomycin or saline (NaCl) as a control and further processed as described.

(B) Total RNA was isolated from the skin, and Cxcl4 mRNA expression was quantified by qPCR (n = 8 per group).

(C) Serum measurement of CXCL4 after treatment with bleomycin or NaCl after the indicated time points was determined by ELISA (n = 7–8 per group).

(D) Representative skin histology analysis after bleomycin or NaCl treatment, stained with Masson trichrome (blue for collagen).

(E) Quantification of (left panel) caliper-measured skin thickness or (right panel) histologically-measured dermal thickness (n = 4–7 per group).

(F) Collagen content upon bleomycin treatment in skin after bleomycin was measured by hydroxyproline assay (n = 5 per group).

(G and H) Representative histological analysis for α-SMA^{+} immune cells in the dermis (G) and their quantification (H) after bleomycin or NaCl control treatment (n = 8 per group).

(I and J) Skin was digested after weeks of treatment, and harvested cells were cultured at 37°C for a week for assessment of dermal myofibroblasts. Shown are representative images of α-SMA-expressing myofibroblasts (I; red) and quantification of α-SMA normalized to cell number by nucleus staining (J; DAPI, blue) (n = 5 per group).

(K–N) WT mice were injected subcutaneously with bleomycin or NaCl control or with an anti-CXCL4 antibody. Shown are representative skin histology analysis after bleomycin only or with additional anti-CXCL4 antibody treatment, stained with Masson trichrome (blue for collagen) (K), quantification of histologically measured dermal thickness (n = 3–6 per group) (L), and representative histological analysis for α-SMA^{+} cells in the dermis (M) and quantification (N) after bleomycin treatment with or without anti-CXCL4 antibodies (n = 3 per group).

(O and P) WT, *Cxcl4*$^{-/-}$, or huCXCL4^{+} mice were treated with bleomycin, and (O) skin thickness was measured with calipers and (P) collagen was measured by hydroxyproline assay (n = 5 per group).

Bars represent mean ± SD. Scale bars, 100 μm. One-way ANOVA with false discovery rate (FDR) correction for multiple testing or two-tailed t test was used. *adj. $p < 0.05$, **$p < 0.01$, ***$p < 0.001$, ****$p < 0.0001$.

CXCL4 (Cochain et al., 2018; Yeo et al., 2016). Using publicly available single-cell RNA sequencing (scRNA-seq) datasets (Figure S1E), we sought to determine the source of CXCL4 in other fibrotic conditions. In a reanalysis of a bleomycin-induced pulmonary fibrosis model (GEO: GSE104154; Xie et al., 2018), we first resolved clusters of immune cells in the lungs using Seurat and Uniform Manifold Approximation and Projection (UMAP) clustering algorithm (Figures S1F and S1G). We identified *Pf4*-expressing cells within the monocytic/macrophage clusters based on their *Cd68* and *Lyz2* expression (clusters 2, 6, 11, 13, and 16). Focusing on these clusters, the highest *Pf4* (encoding CXCL4) expression was found in cluster 16 (Figures S1G and S1H). Cluster 16 expressed high C1q molecules, major histocompatibility complex (MHC) class II molecules, and *Ms4a7* (Figure S1H) and has been classified previously as interstitial macrophages (Joshi et al., 2020). Similarly, in a model of asbestos-induced lung fibrosis (GEO: GSE127803; Joshi et al., 2020), macrophages co-expressing *Pf4* and C1q molecules were also found (cluster 10; Figures S1K–S1M). Remarkably, the numbers of these *Pf4*-expressing cells were increased among macrophages (Figures S1I, S1J, S1N, and S1O). In a study using pressure overload TAC mice (GEO: GSE122930; Martini et al., 2019), *Pf4* expression was also observed in macrophages co-expressing C1q molecules (clusters 11 and 13; Figures S2A–S2D). In this model, these macrophages were described to have an M2-like signature, and their proportions were increased in TAC compared with sham mice after 1 week (Martini et al., 2019).

We further examined CXCL4 expression in human lung fibrosis conditions using two scRNA-seq datasets of individuals with SSc- or non-SSc-associated pulmonary fibrosis (GEO: GSE128169; GEO: GSE135893; Habermann et al., 2020; Valenzi et al., 2019). Focusing on *PTPRC*$^+$ immune cells, we were able to detect the *PF4* transcript among macrophages based on their *CD68*, *CD163*, and *MRC1* expression (Figures S2E–S2H). These findings suggest that macrophages are the potential source of CXCL4 in mouse models of lung and heart fibrosis and in individuals with pulmonary fibrosis.

CXCL4 deficiency abrogates fibrosis in the skin and lungs

We next aimed to elucidate the role of CXCL4 in bleomycin-induced fibrosis development using *Cxcl4*$^{-/-}$ mice. Subcutaneous injection of bleomycin led to the anticipated skin thickening and increase of dermal thickness in wild-type (WT) C57BL/6 mice, whereas in the *Cxcl4*$^{-/-}$ counterparts, the effects of bleomycin were abrogated almost fully (Figures 1D and 1E). In line with these observations, the amount of bleomycin-induced collagen in the skin was reduced significantly in *Cxcl4*$^{-/-}$ mice (Figure 1F). The increase in dermal myofibroblasts (α-SMA$^+$) was also diminished in *Cxcl4*$^{-/-}$ mice, indicating that myofibroblast formation during fibrosis is inhibited in *Cxcl4*-deficient mice (Figures 1G and 1H). Furthermore, *ex vivo* cultures of dermal fibroblasts isolated from bleomycin-treated skin revealed a higher expression level of α-SMA in WT mice compared with *Cxcl4*$^{-/-}$ mice (Figures 1I and 1J). These data suggest that CXCL4 deficiency protects mice from bleomycin-induced skin fibrosis.

CXCL4 promotes inflammatory and fibrotic processes

Next, we further investigated the mechanisms that conferred protection to *Cxcl4*$^{-/-}$ mice against bleomycin exposure. We found increased mRNA expression of the ECM components *Col1a1* and *Col3a1* and the pro-fibrotic *Tgfb1* in the skin of WT mice following bleomycin treatment. The increases in these pro-fibrotic factors were abolished in *Cxcl4*$^{-/-}$ mice (Figure S3A). Decreases in pSMAD2/3 expression in the skin of *Cxcl4*$^{-/-}$ mice following bleomycin treatment was found compared with WT mice (Figures S3B and S3C), indicating that TGF-β signaling might be affected. With respect to inflammation, the number of skin-infiltrating CD45$^+$ immune cells recruited after bleomycin treatment was decreased drastically in *Cxcl4*$^{-/-}$ mice (Figures S3D and S3E). As observed in SSc, bleomycin-treated WT mice showed systemic signs of inflammation, such as increased levels of circulating E-selectin, P-selectin, and the chemokine CXCL1/KC (the murine homologue of IL-8), which were reduced in the *Cxcl4*$^{-/-}$ counterparts (Figure S3F). Furthermore, it has been proposed that pericytes link vascular damage to fibrosis in individuals with SSc via their *trans*-differentiation into myofibroblasts (Rajkumar et al., 2005). We found a high number of PDGFR-β^+ pericytes in the skin of bleomycin-treated WT mice (Figures S3G and S3H). To the contrary, *Cxcl4*$^{-/-}$ mice displayed significantly reduced numbers of pericytes, more resembling control, NaCl-treated WT mice (Figures S3G and S3H). These findings further support a crucial role of CXCL4 in fibrosis development through multiple mechanisms.

CXCL4 blockage ameliorates and CXCL4 overexpression aggravates fibrosis in bleomycin-induced skin fibrosis

Because CXCL4 mediated bleomycin-induced inflammatory and fibrotic processes, we next determined the potential therapeutic effect of blocking CXCL4 using a monoclonal antibody. Remarkably, when mice were administered anti-CXCL4, the increase in dermal thickness after bleomycin treatment was completely suppressed (Figures 1K and 1L), concomitant with reduced numbers of α-SMA$^+$ myofibroblasts (Figures 1M and 1N). This strongly suggests that blocking CXCL4 inhibits fibrosis development induced by bleomycin.

Additionally, to confirm the detrimental fibrotic properties of CXCL4, we used mice deficient in mouse CXCL4 but overexpressing human CXCL4 (hu*CXCL4*$^+$). In these huCXCL4 mice, we found a significant increase in skin fibrosis compared with WT and *Cxcl4*$^{-/-}$ mice following 2 weeks of bleomycin treatment, as demonstrated by skin collagen content and skin thickness measurements (Figures 1O and 1P). Of note, untreated hu*CXCL4*$^+$ mice did not spontaneously develop skin fibrosis, implying that CXCL4 alone is not sufficient to develop fibrosis (data not shown).

CXCL4 deficiency abrogates heart fibrosis

Further support for the role of CXCL4 in fibrosis was sought in the non-SSc-related pressure-overload TAC model *in vivo* (Figure S4). Collagen accumulation appeared in the perivascular and interstitial regions of the heart from WT mice 7 days after TAC, as revealed by trichrome staining, whereas almost none was observed in the *Cxcl4*$^{-/-}$ counterparts (Figure 2A). Moreover, the myofibroblast markers α-SMA and collagen I were

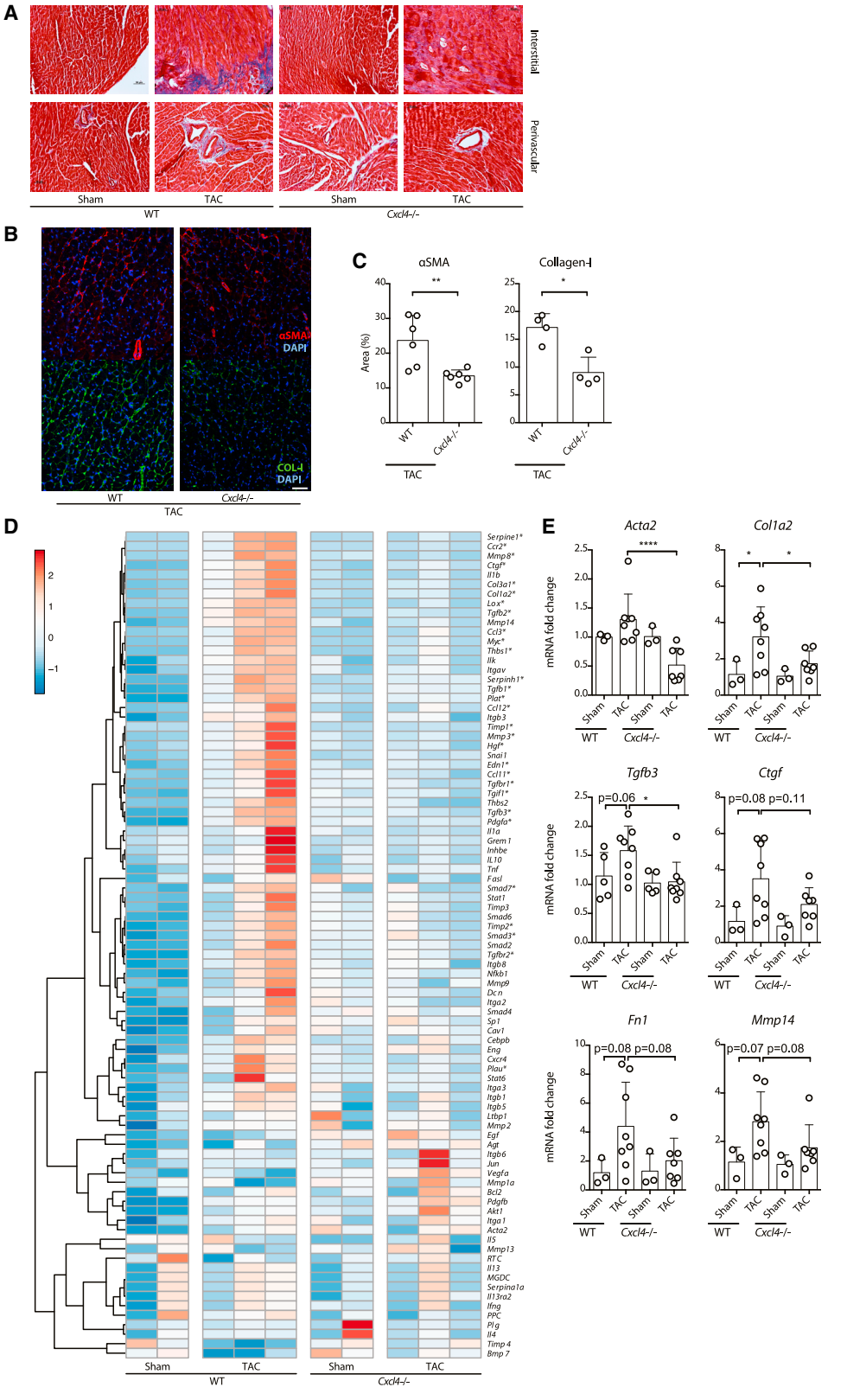

(legend on next page)

decreased significantly in *Cxcl4*$^{-/-}$ mice compared with WT mice after TAC (Figures 2B and 2C). Next, gene expression profiling of fibrosis-associated genes revealed overexpression of genes involved in ECM synthesis and processing (*Acta2*, *Fn1*, *Col1a2*, *Col3a1*, *Mmp14*, and *Lox*), TGF-β signaling (*Tgfb3*, *Ctgf*, *Thbs1*, and *Serpine1*), and the Smad pathway in the hearts of TAC-treated WT mice but not in *Cxcl4*$^{-/-}$ mice (Figures 2D and 2E). Thus, fibrosis development in the TAC model is also mediated by the increase in CXCL4.

The cell-cell interactome reveals that CXCL4 mainly affects fibroblasts and endothelial cells in bleomycin-induced lung fibrosis

Subcutaneous bleomycin treatment is known to induce a systemic inflammatory and fibrotic process in distal organs (Liang et al., 2015). Commensurate with these observations, the lungs of *Cxcl4*$^{-/-}$ mice were almost completely protected against bleomycin-induced fibrosis (Figures 3A and 3B), suggesting that CXCL4 deficiency protects mice from bleomycin-induced skin and lung fibrosis. To predict the cell types involved with CXCL4 in fibrosis models, we performed an unbiased cell-cell interaction analysis, based on a ligand-receptor expression analysis using Connectome (Raredon et al., 2019), on an scRNA-seq dataset of bleomycin-induced lung fibrosis (Xie et al., 2018). We further resolved major cell types in immune and non-immune compartments (Figures 3C, 3D, S5A, and S5B), similar to a previous analysis (Joshi et al., 2020). Upon applying the Connectome network analysis, focusing on cell-cell communication involving *Pf4*, we discovered strong interactions between *Pf4* produced by macrophages (Figure 3E, cluster 16) and receptors expressed on endothelial cells (cluster 10), fibroblasts (clusters 3, 5, and 8), and alveolar type 2 cells (cluster 15) but not other cell types (Figure 3E). We then focused on the interactions between *Pf4*-expressing macrophages and fibroblasts or endothelial cells because they could potentially contribute directly to the fibrotic process. The resulting connectome revealed multiple ligand-receptor interactions between these cells, including *Pf4* (Figure 3F). Similar findings were made in the asbestos-induced lung fibrosis dataset (Figure S5C–S5E; Joshi et al., 2020). This suggests that CXCL4 can directly influence fibroblast and endothelial cells under fibrotic conditions.

CXCL4 stimulates myofibroblast transition of human skin stromal cells

To validate which cell types are involved in CXCL4-driven fibrotic processes, we assessed the role of CXCL4 in myofibroblast differentiation in a variety of primary human precursor cells *in vitro*. First we determined whether CXCL4 had an effect on human skin-derived stromal cells by separating the dermis and adipose layer from normal human skin to isolate dermal fibroblasts and adipose-derived stromal cells (ASCs), respectively (Figure 4A). We cultured these cells with CXCL4 and tested changes in the contractile properties of these cells using a gel contraction assay. After 7 days of culture, CXCL4-treated ASCs induced a higher gel contraction compared with control medium (Figure 4D–4F), but only minimal changes were seen on dermal fibroblasts (Figures 4B and 4C). This CXCL4-induced contractility was maintained until at least 14 days of culture. This was accompanied by increased expression of the myofibroblast markers α-SMA (*ACTA2*), smooth muscle 22 alpha (SM22α/*TAGLN*), and collagen I (*COL1A1*) upon CXCL4 exposure (Figures 4G and S6). These findings reveal that CXCL4 clearly induced a myofibroblast-like phenotype in ASCs.

We then determined collagen production by normal human dermal fibroblasts in a collagen deposition assay. CXCL4 treatment led to an increased amount of deposited collagen by fibroblasts compared with control medium (Figures 4H and 4I). Furthermore, expression of the myofibroblast markers α-SMA (*ACTA2*), SM22α/*TAGLN*, collagen I, and vimentin was increased by CXCL4 in most donor fibroblasts (Figures 4J–4L). However, the effects were modest, and CXCL4 seems to only partially promote transition from fibroblasts to myofibroblasts.

CXCL4 stimulates pericyte-mesenchymal transition and impairs tubule formation in pericyte-endothelial cell co-culture

Pericytes, which function as vessel-associated (mural) support cells, have been theorized to be myofibroblast progenitors in fibrotic processes in different organs (Sundberg et al., 1996). Because we observed increased numbers of pericytes after bleomycin treatment (Figure S3), we further assessed the effect of CXCL4 on human primary pericytes. Pericytes treated with CXCL4 displayed increased RNA and protein expression of the myofibroblast markers α-SMA, SM22α, and collagen I (Figures 5A and 5B). The expression of *FLI1*, a main regulator of ECM production, was also downregulated in pericytes in response to CXCL4 (Figure 5A). These data indicate that CXCL4 induces pericyte-mesenchymal transition and production of collagen by these cells.

By directly interacting with endothelial cells, pericytes play an important role in blood vessel maintenance under homeostatic conditions (Ferland-McCollough et al., 2017). Because EndMT

Figure 2. CXCL4 is required for TAC-induced cardiac fibrosis

WT C57BL/6 or *Cxcl4*$^{-/-}$ mice were subjected to transverse aortic constriction (TAC) or sham surgery (sham).

(A) Representative histological analysis of the heart by Masson trichrome staining (collagen is represented in blue) (sham, n = 3; TAC, n = 8).

(B) Representative histological analysis of α-SMA^{+} myofibroblasts (red), collagen (green), and nucleus staining (DAPI, blue) in the dermis after TAC or sham control treatment.

(C) Quantification of myofibroblasts and collagen (n = 4–6 per group).

(D and E) Total RNA was isolated from the heart after TAC or sham surgery, and mRNA expression was quantified by qPCR. A qPCR array of fibrotic genes from representative mice (sham, n = 2; TAC, n = 3; each from WT and *Cxcl4*$^{-/-}$ mice) was performed (D). Significantly upregulated genes in the WT TAC group compared with WT sham group are indicated by asterisks. Genes were clustered using correlation distance with complete linkage by ClustVis. Single qPCR of selected genes in an enlarged cohort was performed to validate the identified genes (sham, n = 3; TAC, n = 7–8) (E).

Bars represent mean ± SD. Scale bars, 50 μm. One-way ANOVA with FDR correction for multiple testing or two-tailed t test was used, as appropriate. *adj. $p < 0.05$, **$p < 0.01$, ***$p < 0.001$.

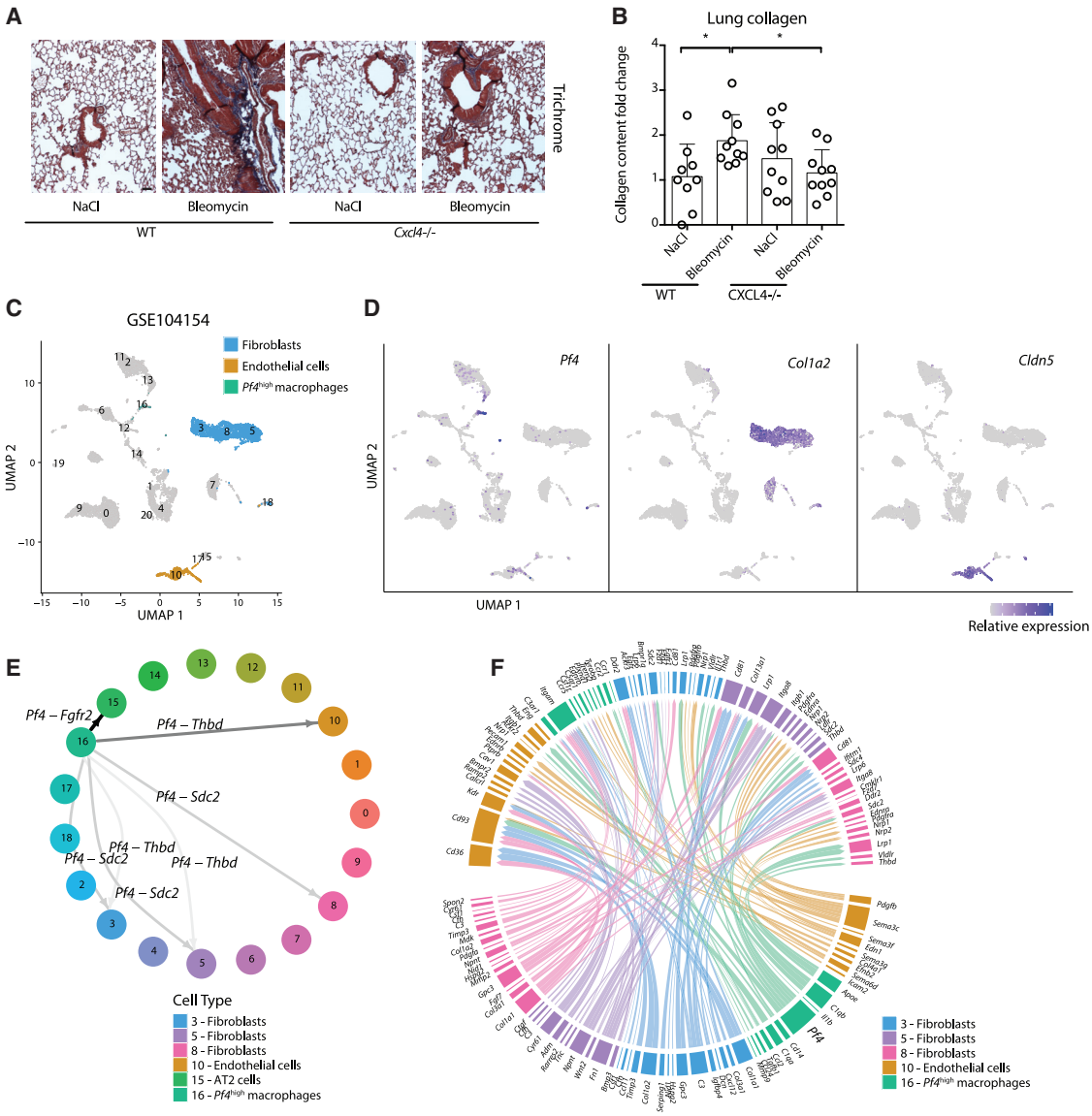

Figure 3. CXCL4 is required for bleomycin-induced lung fibrosis, and Connectome analysis predicts interaction with fibroblasts and endothelial cells

(A) Representative lung histological analysis stained with Masson trichrome.

(B) Collagen content in the lungs after bleomycin exposure was measured by hydroxyproline assay (n = 9–10 per group). Bars represent mean ± SD. Scale bar, 50 μm. One-way ANOVA with FDR correction for multiple testing was used. *adj. $p < 0.05$.

(C and D) Visualization of Pf4^{high} macrophages, fibroblasts, and endothelial cells, identified in scRNA-seq of the bleomycin-induced lung fibrosis dataset, projected onto (C) UMAP space based on expression of (D) Pf4, Col1a2, and Cldn5, respectively.

(E) We mapped vectors of ligand-receptor signaling using Connectome, based on literature-supported ligands and cell surface receptors curated in the FANTOM5 database. When a cognate ligand-receptor pair was greater than 5% of cells, an edge connecting two clusters was created, and weight was calculated as the sum of the two scaled expression values. A network plot involving CXCL4 reveals the connection between Pf4^{high} macrophages (cluster 16) with endothelial cells (cluster 10) and fibroblasts (clusters 3, 5, and 8) and alveolar type 2 (AT2) cells (cluster 15).

(F) Visualization of the connectome using a circos plot of all ligand-receptor interactions between Pf4^{high} macrophages (cluster 16) and endothelial cells (cluster 10) and fibroblasts (clusters 3, 5, and 8).

has also been shown to coincide with increased endothelial cell migration and loss of capillary formation (Lee et al., 2013; Zhang et al., 2013), we sought to investigate the effect of CXCL4 in angiogenesis using pericyte-endothelial cell co-culture to evaluate endothelial cell tubule formation. Addition of CXCL4 drastically reduced the number as well as the length of the tubules formed by endothelial cells in a dose-dependent manner (Figures 5C–5E). Consistent with previous reports (Vandercappellen et al., 2010), increased levels of CXCL4 impaired the endothelial capacity to form an appropriate tissue vasculature.

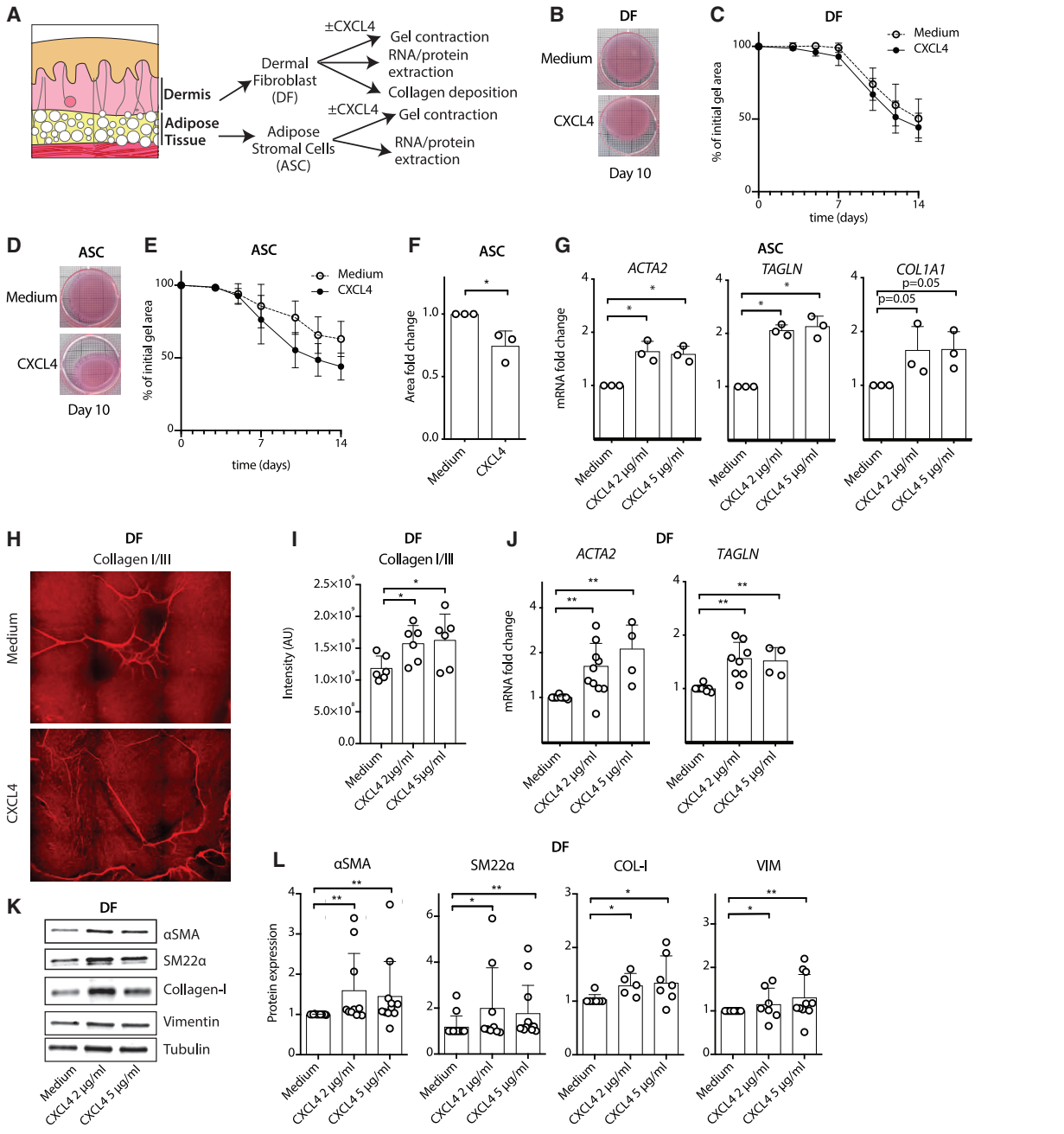

Figure 4. CXCL4 induces a myofibroblast phenotype in primary normal human adipose-derived stromal cells (ASCs) and dermal fibroblasts

(A) Human skin was processed, and ASCs and dermal fibroblasts (DFs) were isolated for further treatment with CXCL4.

(B–E) ASCs or fibroblasts were cultured in collagen gel matrix in the presence or absence of 5 μg/mL CXCL4 for the indicated times, and the area of the gel was measured for contractility (n = 3 per group).

(F) Quantification of the contracted area normalized to control for ASCs on day 14 (n = 3 per group).

(G) ASCs were stimulated with different doses of CXCL4 for 24 h, mRNA was isolated, and gene expression was quantified using qPCR (n = 3 per group).

(H and I) Fibroblasts were cultured in the presence or absence of 5 μg/mL CXCL4 for 7 days. Then cells were lysed, and ECM deposited on the culture vessel was imaged using immunofluorescence. Representative images are shown (H), and collagen I/III amounts, as measured by intensity, were quantified (I) (n = 6 per group).

(J) Fibroblasts were stimulated with different doses of CXCL4 for 24 h, mRNA was isolated, and gene expression was quantified using qPCR (n = 4–10 per group).

(K and L) Fibroblasts were stimulated with different doses of CXCL4 for 24 h. Whole-cell lysate was isolated, and protein expression was assessed by western blot analysis (n = 7–12 per group). Representative images (K) are shown, and the protein level (L) was quantified.

Bars represent mean ± SD. One-way ANOVA with FDR correction for multiple testing was used. *adj. $p < 0.05$, **$p < 0.01$, ***$p < 0.001$, ***$p < 0.0001$.

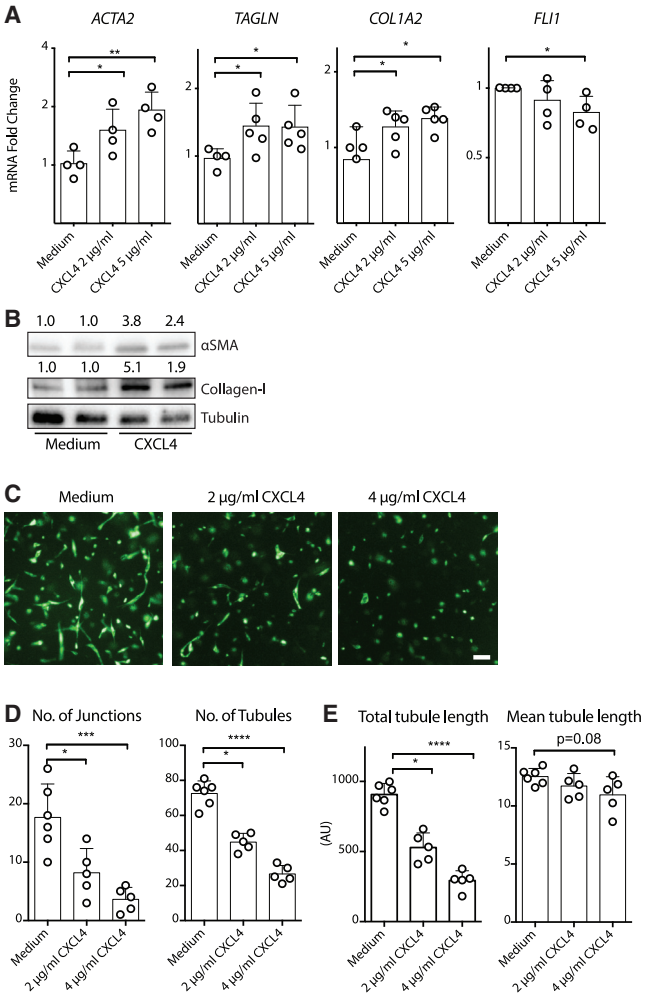

Figure 5. CXCL4 induces myofibroblast differentiation in human pericytes and reduces endothelial cell tubule formation in 3D co-culture with pericytes

(A and B) Normal human brain pericytes were cultured in the presence or absence of CXCL4 for 24 h and processed for RNA and protein analyses.

(A) Total RNA was isolated, and gene expression was quantified using qPCR (n = 4 per group).

(B) Whole-cell lysate was isolated, and protein expression was assessed by western blot analysis. Values from densitometry analysis normalized to tubulin are shown (n = 3–4 per group).

(C–E) Human umbilical vein endothelial cells (HUVECs) transduced with green fluorescent protein were co-cultured with human brain pericytes in a collagen matrix.

(C) After 48-h stimulation with CXCL4 or medium alone, images were acquired. Representative images from 1 of 3 experiments are shown.

(D and E) Endothelial cell tubule formation was quantified by assessment of numbers of junctions and tubules, total length of all tubules, and mean length of the formed tubules (n = 5–6 per group).

Bars represent mean ± SD. Scale bar, 50 μm. One-way ANOVA with FDR correction for multiple testing was used. *adj. $p < 0.05$, **$p < 0.01$.

CXCL4 induces a myofibroblast phenotype in human endothelial cells via metabolic reprogramming

EndMT is a common occurrence in fibrotic conditions (Hinz et al., 2007; Kovacic et al., 2012; Mack and Yanagita, 2015; Piera-Velazquez and Jimenez, 2012). CXCL4 has been shown previously to inhibit endothelial cell proliferation and expression of FLI1 (van Bon et al., 2014a; Dubrac et al., 2010), a main regulator of ECM production and suppressor of EndMT. Hence, we postulated that CXCL4 could directly promote fibrosis by promoting EndMT. After bleomycin treatment, we observed a significant reduction in the number of lectin$^+$α-SMA$^+$ cells in *Cxcl4*$^{-/-}$ mice compared with WT mice, indicating a decrease in EndMT in the absence of CXCL4 (Figures 6A, 6B, and S7).

To better understand the role of CXCL4 in EndMT, we treated human pulmonary arterial endothelial cells with CXCL4 and analyzed transcriptional changes using a qPCR fibrosis array. Expression of the myofibroblast marker α-SMA (*ACTA2*), collagens (*COL1A2* and *COL3A1*), and pro-fibrotic/TGF-β pathways (*SERPIN1* and *TGFB2*) was increased after CXCL4 treatment (Figure 6C). We further confirmed CXCL4-induced upregulation of myofibroblast markers such as α-SMA, SM22α, and collagen I at the RNA (Figure 6D) and protein levels (Figures 6E and 6F). Additionally, changes in cell morphology were observed when endothelial cells were treated with CXCL4, with many cells acquiring a fibroblast-like spindle shape (Figure 6G). Moreover, addition of CXCL4 also reduced expression of the collagen-negative regulator FLI1 (Figures 6D and S6) and increased expression of *COL4A1* and *SNAI1*, a key transcription factor in EndMT (Kokudo et al., 2008; Figure 6D). There were no significant changes in expression of the endothelial cell lineage marker *CDH1* upon CXCL4 treatment (data not shown). These data demonstrate that CXCL4 mediates EndMT and the subsequent increase in collagen synthesis. Furthermore, metabolic changes have been shown to occur during the EndMT process (Xiong et al., 2018). Here we found that endothelial cells treated with CXCL4 had an increased oxygen consumption rate (OCR) compared with control medium (Figures 6H and 6I). Blocking oxidative phosphorylation with oligomycin inhibited expression of myofibroblast markers such as α-SMA and collagen I upon CXCL4 treatment (Figure 6J). In contrast, blocking glycolysis with 2-deoxy-D-glucose (2DG) did not suppress expression of myofibroblast markers. These data indicate that oxidative phosphorylation is required for CXCL4-induced EndMT.

DISCUSSION

Fibrosis is a process that is initiated by soluble factors produced by immune cells that, when uncontrolled, disrupts the original tissue architecture and leads to organ dysfunction, as observed in many chronic inflammatory diseases, such as SSc (Hinz et al., 2012). It is thought that TGF-β is the principal mediator of fibrosis formation, but earlier attempts targeting TGF-β were unsuccessful in fibrotic diseases; only recently has a new pan-TGF-β-neutralizing antibody shown some clinical benefits in individuals with SSc (Lafyatis, 2014; Rice et al., 2015). More recently, IL-11, TLR signaling, and neutrophil extracellular traps have been identified as novel components in fibrosis (Bhattacharyya and Varga, 2017; Martinod et al., 2017; Schafer et al., 2017). Because effective therapies for fibrotic diseases are still lacking (Rockey et al., 2015), the discovery of factors driving fibrogenesis is crucial for development of new therapeutic modalities. Here we identify CXCL4 as a key component in fibrosis

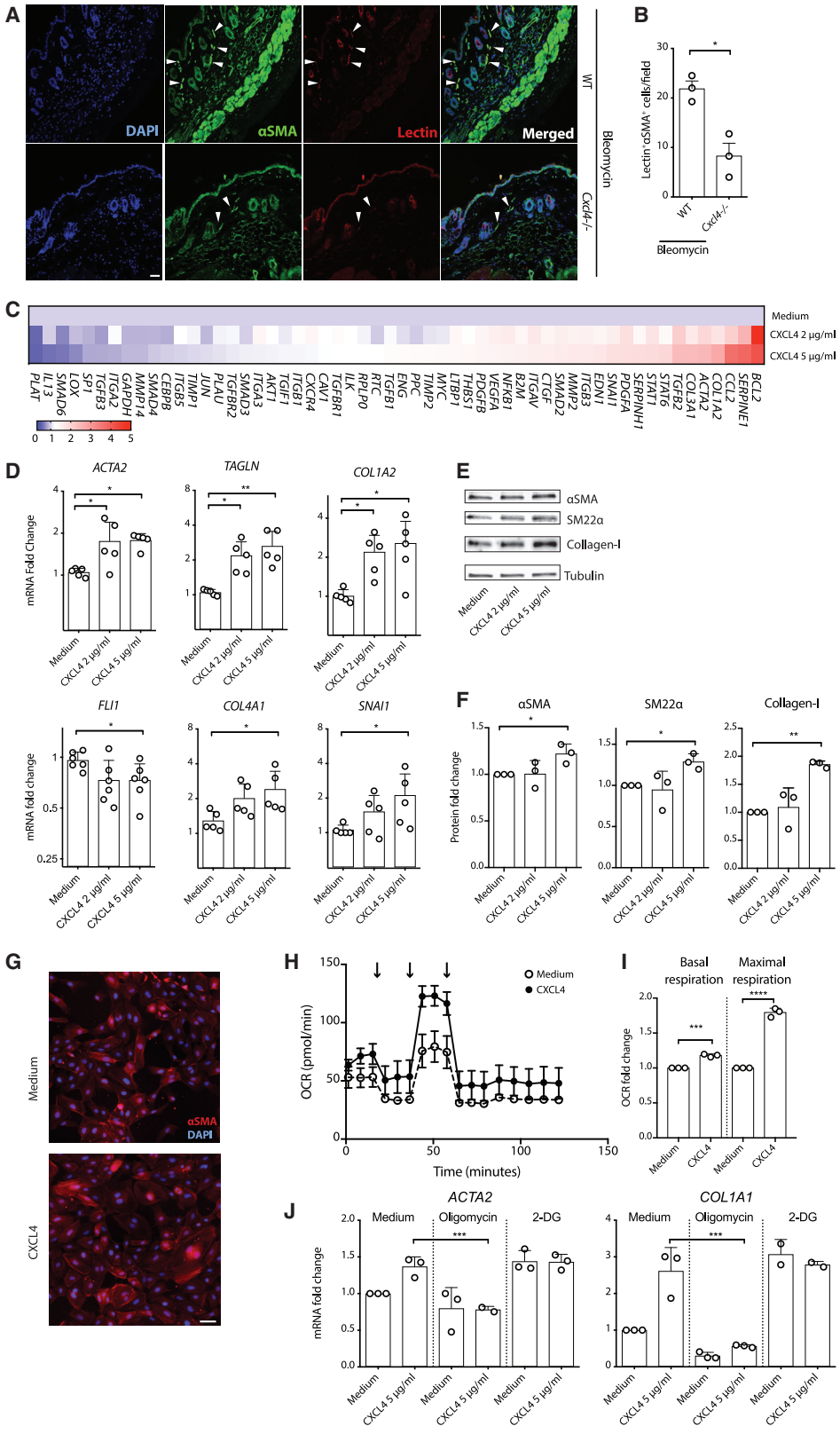

(legend on next page)

development, and we demonstrate a proof of concept of targeting CXCL4 in fibrotic diseases.

We observed an increase in CXCL4 in multiple mouse models of inflammation and fibrosis, including bleomycin- and TLR-induced SSc, Scl-GvHD, and TAC-mediated fibrosis models. The exact mechanism responsible for this pathological increase in CXCL4 is still unknown, although TLR triggering and inflammasome activation may be involved (Ah Kioon et al., 2018; Schaffner et al., 2005; Vandercappellen et al., 2007). More recently, CXCL4 has been shown to be increased in a newly developed mouse model of skin and lung fibrosis, using dendritic cells loaded with topoisomerase I autoantigen, as well as in a bleomycin model (Ah Kioon et al., 2018; Mehta et al., 2016). Our knockout study revealed that mice deficient in CXCL4 are protected from bleomycin-induced skin and lung fibrosis. Moreover, transgenic overexpression of human CXCL4 aggravated bleomycin-induced skin fibrosis. Because bleomycin treatment is a widely used pre-clinical model in research related to dermal and lung fibrosis (Beyer et al., 2010; Williamson et al., 2015), this provides evidence that CXCL4 is a crucial determinant of fibrosis in these diseases.

In the bleomycin model, the presence of inflammation, in particular early in the disease, is needed for fibrosis development. We reported previously that subcutaneous CXCL4 administration led to an increase in $CD45^+$ immune cells (van Bon et al., 2014a), and, remarkably, we found a major reduction of immune cells in the skin of *Cxcl4*$^{-/-}$ mice compared with WT mice following bleomycin injections. Additionally, CXCL4 has the capacity to promote inflammation by amplifying TLR signaling of innate and adaptive immune cells (van Bon et al., 2014a; Lande et al., 2019; Silva-Cardoso et al., 2017) and by inducing chemokine production by monocytes (van der Kroef et al., 2020). These data indicate that the presence of CXCL4 is crucial for chemotaxis of immune cells toward the site of injury, and this reveals another layer of possible mechanisms by which CXCL4 leads to fibrosis development.

In addition to the bleomycin model, we demonstrate that CXCL4 is also required for development of TAC-induced heart fibrosis. Cardiac involvement is the second leading cause of death after pulmonary complications in individuals with SSc (Tyndall et al., 2010). The pathogenic role of CXCL4 has been shown in atherosclerosis and ischemia/reperfusion models (Koenen et al., 2009; Lapchak et al., 2012). Although the absence of CXCL4 ameliorated TAC-induced fibrosis, we did not observe any improvement in heart function, suggesting involvement of other cytokines in other aspects of the disease. Interestingly, exogenous CXCL4 administration has been shown to exacerbate left ventricular (LV) dilation, leading to increased mortality, in a mouse coronary artery ligation-induced myocardial infarction model (Lindsey et al., 2019). However, the role of CXCL4 in coronary artery disease remains unclear (Erbel et al., 2015; Levine et al., 1981), and CXCL4 contribution to cardiac fibrosis development in humans still needs to be verified. The pro-fibrotic role of CXCL4 has also been shown in other tissues. In a thrombopoietin-induced myelofibrosis model, the absence of CXCL4 in hematopoietic stem and progenitor cells reduced bone marrow fibrosis (Gleitz et al., 2020). Upon treatment with CCl_4 or thioacetamide, *Cxcl4*$^{-/-}$ mice showed amelioration of liver fibrosis (Zaldivar et al., 2010). In a rat model of chronic liver allograft dysfunction, blocking CXCL4 could significantly protect rats from liver fibrosis (Li et al., 2016). In this study, we demonstrate that blocking CXCL4 effectively abrogates bleomycin-induced skin fibrosis. Additionally, we did not observe any adverse events in mice treated with anti-CXCL4; thus, systemic targeting of CXCL4 using monoclonal antibodies should be considered and evaluated carefully in future studies. Our data on experimental models of skin, lung, and cardiac fibrosis further corroborate the notion of CXCL4 as a central mediator of fibrosis *in vivo* and a potential therapeutic target.

Myofibroblasts, as identified by high expression of α-SMA and production of ECM proteins, is a defining feature of tissue fibrosis. Although it was initially thought that resident fibroblasts were the source of myofibroblasts, it is becoming clear that they can be derived from multiple precursors, including endothelial cells and pericytes (Hinz et al., 2007, 2012; Ho et al., 2014; Mack and Yanagita, 2015). Here we demonstrated that CXCL4 induced myofibroblast-like properties in endothelial cells, pericytes, ASCs, and dermal fibroblasts. In the bleomycin model, the majority of α-SMA^+ myofibroblasts have been shown to express pericyte markers (Liu et al., 2010). Our *in vivo* data are in line with these findings, showing that pericytes were present

Figure 6. CXCL4 stimulates myofibroblast differentiation in endothelial cells via metabolic changes

(A and B) Skin from WT C57BL/6 or *Cxcl4*$^{-/-}$ mice injected with bleomycin was stained for α-SMA^+ myofibroblasts (green), lectin (red), and nucleus staining (DAPI, blue). Shown are (A) representative immunostaining and quantification of lectin$^+$ α-SMA^+ cells (B).

(C–J) Normal human pulmonary endothelial cells (HPAECs) were cultured in the presence or absence of CXCL4 for 24 h and processed for RNA, protein, and metabolic analyses.

(C and D) Total RNA was isolated, and gene expression was determined using (C) a qPCR fibrosis array (n = 3 per group) and further validated by (D) qPCR by including additional experiments (n = 5 per group).

(E and F) Whole-cell lysates were isolated, and protein expression was assessed by western blot analysis. Shown are a representative blot (E) and quantification (F) (n = 3 per group).

(G) HPAECs were cultured in the presence or absence of CXCL4 for 24 h and fixed and permeabilized prior to staining of α-SMA (red) and nuclei (Hoechst, blue). Representative immunofluorescence images from one of 3 independent experiments are shown.

(H and I) After 24-h CXCL4 (open circle) or control (closed circle) treatment, HPAECs were cultured in XF basal medium, and OCR was measured in response to oligomycin, FCCP, and rotenone, as indicated by the arrows. Shown are representative OCR measurements and quantification of basal and maximal respiration (I).

(J) HPAECs were cultured in the presence or absence of CXCL4, 1 μM oligomycin, and 100 mM 2DG for 24 h. RNA was isolated, and gene expression was quantified using qPCR (n = 2–3 per group).

Bars represent mean ± SD. Scale bars, 50 μm. One-way ANOVA with FDR correction for multiple testing or two-tailed t test was used, as appropriate. *adj. $p < 0.05$, **$p < 0.01$, ***$p < 0.001$, ****$p < 0.0001$.

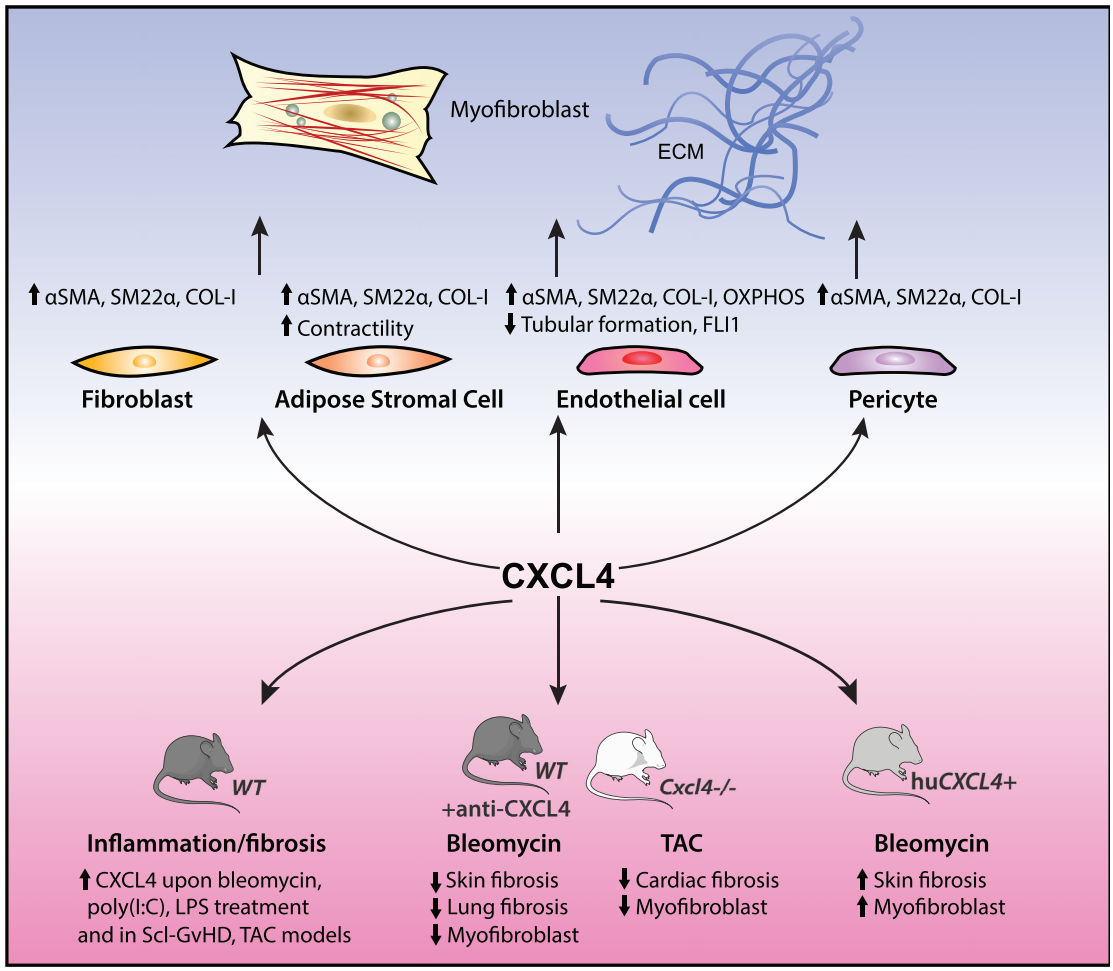

Figure 7. CXCL4 as a key pro-fibrogenic molecule

Using a genetic approach (knockout and overexpression) and a blocking antibody, we show the essential role of CXCL4 in fibrosis development in the skin, lungs, and heart using two independent fibrosis models and the therapeutic potential of targeting CXCL4 against fibrosis. Our study also demonstrates that CXCL4 directly induces myofibroblast differentiation from different precursor cells, including stromal cells and endothelial cells.

in high numbers in fibrotic skin of these mice. To the contrary, in *Cxcl4*$^{-/-}$ mice, pericytes were reduced significantly, more resembling control mice. Increased numbers of activated PDGFR-β^+ pericytes have also been found in fibrotic skin of individuals with SSc (Rajkumar et al., 1999). These activated pericytes were positive for myofibroblast markers such as α-SMA, ED-A splice variant of fibronectin (ED-A FN), and Thy-1 (Rajkumar et al., 2005). The crucial role of pericytes as a source of myofibroblasts in the skin is further supported by another study demonstrating that the majority of collagen-producing α-SMA$^+$ myofibroblasts were generated from a PDGFR-β^+ NG2$^+$ perivascular subpopulation following acute dermal injury (Dulauroy et al., 2012). Our data showed that α-SMA staining of bleomycin-treated skin from *Cxcl4*$^{-/-}$ mice is reduced and that skin fibroblasts isolated from *Cxcl4*$^{-/-}$ mice following bleomycin injection expressed less α-SMA compared with WT mice. Thus, our data suggest that CXCL4 plays a pivotal role in myofibroblast differentiation, in which pericytes were among the source, leading to fibrosis development *in vivo*. This is in line with our *in vitro* observations, where CXCL4 stimulation of pericytes leads to *trans*-differentiation into myofibroblasts.

Adipocytes are another potential source of myofibroblasts, and this has been described in bleomycin-induced SSc models (Marangoni et al., 2015; Martins et al., 2015). In this respect, increased dermal CXCL4 could be one of the factors that drives intradermal fat loss at the expense of increased fibrosis, and this needs further evaluation (Onuora, 2015). We observed that ASCs showed increased myofibroblast markers and acquired contractility when exposed to CXCL4, indicating that these cells also contribute to CXCL4-driven tissue fibrosis. Interestingly, this CXCL4 effect on myofibroblast differentiation was more pronounced in ASCs compared with dermal fibroblasts.

Previously, serum derived from individuals with SSc has been shown to induce EndMT in dermal microvascular endothelial cells (Manetti et al., 2017). Because of the high amount of CXCL4 in the circulation of these individuals (van Bon et al., 2014b; Haddon et al., 2017; Valentini et al., 2017; Volkmann et al., 2016), it is likely that CXCL4 might be a driving force in

MT from cells in the vasculature. We observed a lower number of lectin$^+$ α-SMA$^+$ endothelium-derived myofibroblasts in *Cxcl4*$^{-/-}$ mice upon bleomycin treatment, indicating a role of CXCL4 in inducing EndMT *in vivo*. Indeed, our *in vitro* experiments with endothelial cells confirmed that CXCL4 stimulation directly initiated myofibroblast differentiation and induced collagen synthesis. This was accompanied by a decrease in FLI1, a transcription factor that is crucial for preserving endothelial cell identity, and loss of its expression triggers EndMT (Nagai et al., 2018). FLI1 downregulation can also be mediated by an increase in TGF-β2 and Endothelin-1 (Chrobak et al., 2013); both were increased by CXCL4, although further studies are needed to verify these mechanisms of action. CXCL4-induced EndMT also depends on a metabolic shift to oxidative phosphorylation, confirming previous findings showing that increased OCR is required for myofibroblast differentiation (Bernard et al., 2015; Negmadjanov et al., 2015). Furthermore, CXCL4 is known for its angiogenic effect on endothelial cells (Sarabi et al., 2011). Using 3D co-culture of pericytes and endothelial cells, a system closer to physiological conditions, we confirmed that CXCL4 inhibited endothelial tubule formation. CXCL4 directly promotes EndMT and suppresses vasculogenesis, prominent features of SSc (Trojanowska, 2010).

We present evidence of CXCL4 as a targetable fibrogenic molecule that directly promotes MT in a variety of precursor cells essential for fibrosis development across multiple organs *in vivo* (Figure 7). Furthermore, CXCL4 also plays an important role in mediating innate and adaptive immune responses (Affandi et al., 2018; Gleissner, 2012; Gouwy et al., 2016; Silva-Cardoso et al., 2017), inducing vascular changes (Aidoudi-Ahmed and Bikfalvi, 2010; Van Raemdonck et al., 2014), and it is required in other inflammatory models *in vivo* (Grommes et al., 2012; von Hundelshausen et al., 2017; Koenen et al., 2009; Lapchak et al., 2012). As a key upstream molecule linking multiple processes, CXCL4 is a promising target for intervention in SSc and potentially many other inflammatory and fibrotic disorders.

Limitations of the study

The present study demonstrates the pro-fibrogenic role of CXCL4 in fibroinflammatory models. Although it is clear that absence of CXCL4 almost completely protected mice from developing skin fibrosis in the bleomycin model, it is unclear why heart function was not restored despite amelioration of fibrosis in the TAC model. Furthermore, in the current study, we were not able to investigate diastolic dysfunction using tissue Doppler echocardiography or invasive catheter measurement. Additionally, we did not assess whether CXCL4 deletion could restore respiratory function in the bleomycin model. Although this assessment is not routinely performed in the subcutaneous bleomycin model, the degree of bleomycin-induced fibrosis in the lungs has been shown to correlate well with respiratory function (Phillips et al., 2012). We did observe a significant reduction in lung fibrosis in the absence of CXCL4; however, changes in lung function are unknown. Finally, although our data indicate that CXCL4 may involve TGF-β-SMAD signaling (Figures 2, S3, and 5), the signaling pathways activated by CXCL4 in promoting MT transformation in different cell types requires further investigation.

STAR★METHODS

Detailed methods are provided in the online version of this paper and include the following:

- KEY RESOURCES TABLE
- RESOURCE AVAILABILITY
  - Lead contact
  - Materials availability
  - Data and code availability
- EXPERIMENTAL MODEL AND SUBJECT DETAILS
  - Cell culture
  - Animal experiments
  - Bleomycin-induced skin and lung fibrosis
  - *In vivo* administration of TLR ligands
  - Induction of Scl-GvHD in mice
  - Transverse aortic constriction
- METHOD DETAILS
  - RNA isolation and quantitative PCR
  - Western blotting
  - Extracellular matrix deposition assay
  - Collagen gel contraction assay
  - Endothelial tubule formation assay
  - Metabolic assays
  - Immunofluorescence of mouse fibroblasts *ex vivo*
  - Tissue immunohistochemistry and immunofluorescence
  - Measurement of secreted proteins
  - Histochemical analysis
  - Quantification of tissue collagen
  - Single-cell RNA sequencing analysis
- QUANTIFICATION AND STATISTICAL ANALYSIS

SUPPLEMENTAL INFORMATION

Supplemental information can be found online at https://doi.org/10.1016/j.celrep.2021.110189.

ACKNOWLEDGMENTS

A.J.A. was supported by the Dutch Arthritis Association (Reumafonds grant NR-10-1-301) and the Netherlands Organisation for Scientific Research (NWO, Mosaic grant 017.008.014). T.C. was supported by a grant from the Portuguese National Funding Agency for Science, Research and Technology: Fundação para a Ciência e a Tecnologia [SFRH/BD/93526/2013]. T.R.D.J.R and J.A.G.v.R. received funding from an European Research Council (ERC) Starting Grant (ERC-2011-StG, Circumvent). W.M. obtained funding from the Marie Curie Intra-European Fellowship (Proposal number: 624871) and from the NWO VENI (grant number 91919149). We thank Mike DiMarzio, Giuseppina A. Farina (Boston University School of Medicine), Sarita Hartgring, Aniek Meijers, Karin de Cortie, Wouter van Leeuwen, Dirk-Jan Heijnen, Enric Mocholi-Gimeno, and Christian van Dijk (University Medical Center Utrecht) for technical advice, support, and expertise. We also thank Kris A. Reedquist for critical review of the manuscript.

AUTHOR CONTRIBUTIONS

A.J.A., T.C., T.R.D.J.R., and W.M. conceived the experiments and drafted and revised the manuscript. A.J.A., T.C., C.C., M.A.K., S. Gibbs, S.C.A.d.J., J.A.G.v.R., T.R.D.J.R., and W.M. designed the experiments. A.J.A., T.C., A.O., J.J.d.H., M.A.D.B., M.M.B., R.G.T., A.P.L., B.M.F., C.P.J.B., M.v.d.L., M.Z., B.G., C.G.K.W., S. Garcia, M.d.K., M.W., G.S., and Y.J.X. carried out

the experiments and analyses. C.P.J.B., M.A.K., J.A.G.v.R., S. Garcia, M.W., and S.C.A.d.J. revised the manuscript. J.A.G.v.R., T.R.D.J.R., and W.M. supervised the study. All authors made substantial, direct, and intellectual contributions to the work and approved the final version of the manuscript.

DECLARATION OF INTERESTS

The authors declare no competing interests.

Received: May 15, 2020
Revised: February 28, 2021
Accepted: December 8, 2021
Published: January 4, 2022

REFERENCES

Affandi, A.J., Silva-Cardoso, S.C., Garcia, S., Leijten, E.F.A., van Kempen, T.S., Marut, W., van Roon, J.A.G., and Radstake, T.R.D.J. (2018). CXCL4 is a novel inducer of human Th17 cells and correlates with IL-17 and IL-22 in psoriatic arthritis. Eur. J. Immunol. *48*, 522–531.

Ah Kioon, M.D., Tripodo, C., Fernandez, D., Kirou, K.A., Spiera, R.F., Crow, M.K., Gordon, J.K., and Barrat, F.J. (2018). Plasmacytoid dendritic cells promote systemic sclerosis with a key role for TLR8. Sci. Transl. Med. *10*, 1–14.

Aidoudi-Ahmed, S., and Bikfalvi, A. (2010). Interaction of PF4 (CXCL4) with the vasculature: A role in atherosclerosis and angiogenesis. Thromb. Haemost. *104*, 941–948.

Bernard, K., Logsdon, N.J., Ravi, S., Xie, N., Persons, B.P., Rangarajan, S., Zmijewski, J.W., Mitra, K., Liu, G., Darley-Usmar, V.M., et al. (2015). Metabolic reprogramming is required for myofibroblast contractility and differentiation. J. Biol. Chem. *290*, 25427–25438.

Beyer, C., Schett, G., Distler, O., and Distler, J.H.W. (2010). Animal models of systemic sclerosis: prospects and limitations. Arthritis Rheum. *62*, 2831–2844.

Bhattacharyya, S., and Varga, J. (2017). Endogenous ligands of TLR4 promote unresolving tissue fibrosis: implications for systemic sclerosis and its targeted therapy. Immunol. Lett.

van Bon, L., Affandi, A.J., Broen, J., Christmann, R.B., Marijnissen, R.J., Stawski, L., Farina, G.A., Stifano, G., Mathes, A.L., Cossu, M., et al. (2014a). Proteome-wide analysis and CXCL4 as a biomarker in systemic sclerosis. N. Engl. J. Med. *370*, 433–443.

van Bon, L., Cossu, M., Loof, A., Gohar, F., Wittkowski, H., Vonk, M., Roth, J., van den Berg, W., van Heerde, W., Broen, J.C.A., et al. (2014b). Proteomic analysis of plasma identifies the Toll-like receptor agonists S100A8/A9 as a novel possible marker for systemic sclerosis phenotype. Ann. Rheum. Dis. *73*, 1585–1589.

Burstein, S.A., Malpass, T.W., Yee, E., Kadin, M., Brigden, M., Adamson, J.W., and Harker, L.A. (1984). Platelet factor-4 excretion in myeloproliferative disease: implications for the aetiology of myelofibrosis. Br. J. Haematol. *57*, 383–392.

Butler, A., Hoffman, P., Smibert, P., Papalexi, E., and Satija, R. (2018). Integrating single-cell transcriptomic data across different conditions, technologies, and species. Nat. Biotechnol. *36*, 411–420.

Chen, Y., Yu, Q., and Xu, C.B. (2017). A convenient method for quantifying collagen fibers in atherosclerotic lesions by imagej software. Int. J. Clin. Exp. Med. *10*, 14904–14910.

Chrifi, I., Louzao-Martinez, L., Brandt, M., van Dijk, C.G.M., Burgisser, P., Zhu, C., Kros, J.M., Duncker, D.J., and Cheng, C. (2017). CMTM3 (CKLF-like marvel transmembrane domain 3) mediates angiogenesis by regulating cell surface availability of VE-cadherin in endothelial adherens junctions. Arterioscler. Thromb. Vasc. Biol. *37*, 1098–1114.

Chrobak, I., Lenna, S., Stawski, L., and Trojanowska, M. (2013). Interferon-γ promotes vascular remodeling in human microvascular endothelial cells by upregulating endothelin (ET)-1 and transforming growth factor (TGF) β2. J. Cell. Physiol. *228*, 1774–1783.

Cochain, C., Vafadarnejad, E., Arampatzi, P., Pelisek, J., Winkels, H., Ley, K., Wolf, D., Saliba, A.E., and Zernecke, A. (2018). Single-cell RNA-seq reveals the transcriptional landscape and heterogeneity of aortic macrophages in murine atherosclerosis. Circ. Res. *122*, 1661–1674.

Duan, H., Fleming, J., Pritchard, D.K., Amon, L.M., Xue, J., Arnett, H.a., Chen, G., Breen, P., Buckner, J.H., Molitor, J.a., et al. (2008). Combined analysis of monocyte and lymphocyte messenger RNA expression with serum protein profiles in patients with scleroderma. Arthritis Rheum. *58*, 1465–1474.

Dubrac, A., Quemener, C., Lacazette, E., Lopez, F., Zanibellato, C., Wu, W.-G., Bikfalvi, A., and Prats, H. (2010). Functional divergence between 2 chemokines is conferred by single amino acid change. Blood *116*, 4703–4711.

Dulauroy, S., Di Carlo, S.E., Langa, F., Eberl, G., and Peduto, L. (2012). Lineage tracing and genetic ablation of ADAM12 (+) perivascular cells identify a major source of profibrotic cells during acute tissue injury. Nat. Med. *18*, 1262–1270.

Erbel, C., Korosoglou, G., Ler, P., Akhavanpoor, M., Domschke, G., Linden, F., Doesch, A.O., Buss, S.J., Giannitsis, E., Katus, H.A., et al. (2015). CXCL4 Plasma levels are not associated with the extent of coronary artery disease or with coronary plaque morphology. PLoS One *10*, e0141693.

Eslin, D.E., Zhang, C., Samuels, K.J., Rauova, L., Zhai, L., Niewiarowski, S., Cines, D.B., Poncz, M., and Kowalska, M.A. (2004). Transgenic mice studies demonstrate a role for platelet factor 4 in thrombosis: dissociation between anticoagulant and antithrombotic effect of heparin. Blood *104*, 3173–3180.

Farina, G.A., York, M.R., Di Marzio, M., Collins, C.A., Meller, S., Homey, B., Rifkin, I.R., Marshak-Rothstein, A., Radstake, T.R.D.J., and Lafyatis, R. (2010). Poly(I:C) drives type I IFN- and TGFβ-mediated inflammation and dermal fibrosis simulating altered gene expression in systemic sclerosis. J. Invest. Dermatol. *130*, 2583–2593.

Ferland-McCollough, D., Slater, S., Richard, J., Reni, C., and Mangialardi, G. (2017). Pericytes, an overlooked player in vascular pathobiology. Pharmacol. Ther. *171*, 30–42.

Gleissner, C.a (2012). Macrophage phenotype modulation by CXCL4 in atherosclerosis. Front. Physiol. *3*, 1.

Gleitz, H.F.E., Dugourd, A.J.F., Leimkühler, N.B., Snoeren, I.A.M., Fuchs, S.N.R., Menzel, S., Ziegler, S., Kröger, N., Triviai, I., Büsche, G., et al. (2020). Increased CXCL4 expression in hematopoietic cells links inflammation and progression of bone marrow fibrosis in MPN. Blood *136*, 2051–2064.

Gouwy, M., Ruytinx, P., Radice, E., Claudi, F., Van Raemdonck, K., Bonecchi, R., Locati, M., and Struyf, S. (2016). CXCL4 and CXCL4L1 differentially affect monocyte survival and dendritic cell differentiation and phagocytosis. PLoS ONE *11*, e0166006.

Grommes, J., Alard, J.-E., Drechsler, M., Wantha, S., Mörgelin, M., Kuebler, W.M., Jacobs, M., von Hundelshausen, P., Markart, P., Wygrecka, M., et al. (2012). Disruption of platelet-derived chemokine heteromers prevents neutrophil extravasation in acute lung injury. Am. J. Respir. Crit. Care Med. *185*, 628–636.

de Haan, J.J., Bosch, L., Borgman, A., Bastemeijer, M., Brans, M.A.D., van de Weg, S.M., de Kleijn, D.P.V., Sluijter, J.P.G., el Azzouzi, H., and de Jager, S.C.A. (2017). Complement 5a receptor deficiency does not influence adverse cardiac remodeling after pressure-overload in mice. Sci. Rep. *7*, 17045.

Habermann, A.C., Gutierrez, A.J., Bui, L.T., Yahn, S.L., Winters, N.I., Calvi, C.L., Peter, L., Chung, M.-I., Taylor, C.J., Jetter, C., et al. (2020). Single-cell RNA sequencing reveals profibrotic roles of distinct epithelial and mesenchymal lineages in pulmonary fibrosis. Sci. Adv. *6*, eaba1972.

Haddon, D.J., Wand, H.E., Jarrell, J.A., Spiera, R.F., Utz, P.J., Gordon, J.K., and Chung, L.S. (2017). Proteomic analysis of sera from individuals with diffuse cutaneous systemic sclerosis reveals a multianalyte signature associated with clinical improvement during imatinib mesylate treatment. J. Rheumatol. *44*, 631–638.

Hinz, B., Phan, S.H., Thannickal, V.J., Galli, A., Bochaton-Piallat, M.-L., and Gabbiani, G. (2007). The myofibroblast. Am. J. Pathol. *170*, 1807–1816.

Hinz, B., Phan, S.H., Thannickal, V.J., Prunotto, M., Desmoulire, A., Varga, J., De Wever, O., Mareel, M., and Gabbiani, G. (2012). Recent developments in

myofibroblast biology: Paradigms for connective tissue remodeling. Am. J. Pathol. *180*, 1340–1355.

Ho, Y.Y., Lagares, D., Tager, A.M., and Kapoor, M. (2014). Fibrosis - a lethal component of systemic sclerosis. Nat. Rev. Rheumatol. *10*, 390–402.

von Hundelshausen, P., Agten, S.M., Eckardt, V., Blanchet, X., Schmitt, M.M., Ippel, H., Neideck, C., Bidzhekov, K., Leberzammer, J., Wichapong, K., et al. (2017). Chemokine interactome mapping enables tailored intervention in acute and chronic inflammation. Sci. Transl Med. *9*, 1–15.

de Jager, W., Prakken, B.J., Bijlsma, J.W.J., Kuis, W., and Rijkers, G.T. (2005). Improved multiplex immunoassay performance in human plasma and synovial fluid following removal of interfering heterophilic antibodies. J. Immunol. Methods *300*, 124–135.

Joshi, N., Watanabe, S., Verma, R., Jablonski, R.P., Chen, C.I., Cheresh, P., Markov, N.S., Reyfman, P.A., McQuattie-Pimentel, A.C., Sichizya, L., et al. (2020). A spatially restricted fibrotic niche in pulmonary fibrosis is sustained by M-CSF/M-CSFR signalling in monocyte-derived alveolar macrophages. Eur. Respir. J. *55*, 1900646.

Kabala, P.A., Angiolilli, C., Yeremenko, N., Grabiec, A.M., Giovannone, B., Pots, D., Radstake, T.R., Baeten, D., and Reedquist, K.A. (2017). Endoplasmic reticulum stress cooperates with Toll-like receptor ligation in driving activation of rheumatoid arthritis fibroblast-like synoviocytes. Arthritis Res. Ther. *19*, 1–11.

Kasper, B., Winoto-Morbach, S., Mittelstädt, J., Brandt, E., Schütze, S., and Petersen, F. (2010). CXCL4-induced monocyte survival, cytokine expression, and oxygen radical formation is regulated by sphingosine kinase 1. Eur. J. Immunol. *40*, 1162–1173.

Kavian, N., Marut, W., Servettaz, A., Laude, H., Nicco, C., Chéreau, C., Weill, B., and Batteux, F. (2012). Arsenic trioxide prevents murine sclerodermatous graft-versus-host disease. J. Immunol. *188*, 5142–5149.

Kendall, R.T., and Feghali-Bostwick, C.a. (2014). Fibroblasts in fibrosis: novel roles and mediators. Front. Pharmacol. *5*, 123.

Koenen, R.R., von Hundelshausen, P., Nesmelova, I.V., Zernecke, A., Liehn, E.A., Sarabi, A., Kramp, B.K., Piccinini, A.M., Paludan, S.R., Kowalska, M.A., et al. (2009). Disrupting functional interactions between platelet chemokines inhibits atherosclerosis in hyperlipidemic mice. Nat. Med. *15*, 97–103.

Kokudo, T., Suzuki, Y., Yoshimatsu, Y., Yamazaki, T., Watabe, T., and Miyazono, K. (2008). Snail is required for TGF -induced endothelial-mesenchymal transition of embryonic stem cell-derived endothelial cells. J. Cell Sci. *121*, 3317–3324.

Kovacic, J.C., Mercader, N., Torres, M., Boehm, M., and Fuster, V. (2012). Epithelial-to-mesenchymal and endothelial-to-mesenchymal transition: from cardiovascular development to disease. Circulation *125*, 1795–1808.

van der Kroef, M., Carvalheiro, T., Rossato, M., de Wit, F., Cossu, M., Chouri, E., Wichers, C.G.K., Bekker, C.P.J., Beretta, L., Vazirpanah, N., et al. (2020). CXCL4 triggers monocytes and macrophages to produce PDGF-BB, culminating in fibroblast activation: implications for systemic sclerosis. J. Autoimmun. *111*, 102444.

Kroeze, K.L., Jurgens, W.J., Doulabi, B.Z., van Milligen, F.J., Scheper, R.J., and Gibbs, S. (2009). Chemokine-mediated migration of skin-derived stem cells: predominant role for CCL5/RANTES. J. Invest. Dermatol. *129*, 1569–1581.

Lafyatis, R. (2014). Transforming growth factor β-at the centre of systemic sclerosis. Nat. Rev. Rheumatol.

Lande, R., Lee, E.Y., Palazzo, R., Marinari, B., Pietraforte, I., Santos, G.S., Mattenberger, Y., Spadaro, F., Stefanantoni, K., Iannace, N., et al. (2019). CXCL4 assembles DNA into liquid crystalline complexes to amplify TLR9-mediated interferon-α production in systemic sclerosis. Nat. Commun. *10*, 1731.

Lapchak, P.H., Ioannou, A., Rani, P., Lieberman, L.A., Yoshiya, K., Kannan, L., Dalle Lucca, J.J., Kowalska, M.A., and Tsokos, G.C. (2012). The role of platelet factor 4 in local and remote tissue damage in a mouse model of mesenteric ischemia/reperfusion injury. PLoS One *7*, e39934.

Lee, S.-W., Won, J.-Y., Kim, W.J., Lee, J., Kim, K.-H., Youn, S.-W., Kim, J.-Y., Lee, E.J., Kim, Y.-J., Kim, K.-W., et al. (2013). Snail as a potential target molecule in cardiac fibrosis: paracrine action of endothelial cells on fibroblasts through snail and CTGF axis. Mol. Ther. *21*, 1767–1777.

Levine, S.P., Lindenfeld, J., Ellis, J.B., Raymond, N.M., and Krentz, L.S. (1981). Increased plasma concentrations of platelet factor 4 in coronary artery disease: a measure of in vivo platelet activation and secretion. Circulation *64*, 626–632.

Li, J., Liu, B., Shi, Y., Xie, K., Yin, H., Yan, L., Lau, W., and Wang, G. (2016). CXCL4 contributes to the pathogenesis of chronic liver allograft dysfunction. J. Immunol. Res. *2016*, 9276986.

Liang, M., Lv, J., Zou, L., Yang, W., Xiong, Y., Chen, X., Guan, M., He, R., and Zou, H. (2015). A modified murine model of systemic sclerosis: bleomycin given by pump infusion induced skin and pulmonary inflammation and fibrosis. Lab. Investig. *95*, 342–350.

Lindsey, M.L., Jung, M., Yabluchanskiy, A., Cannon, P.L., Iyer, R.P., Flynn, E.R., Deleon-Pennell, K.Y., Valerio, F.M., Harrison, C.L., Ripplinger, C.M., et al. (2019). Exogenous CXCL4 infusion inhibits macrophage phagocytosis by limiting CD36 signalling to enhance post-myocardial infarction cardiac dilation and mortality. Cardiovasc. Res. *115*, 395–408.

Liu, S., Taghavi, R., and Leask, A. (2010). Connective tissue growth factor is induced in bleomycin-induced skin scleroderma. J. Cell Commun. Signal. *4*, 25–30.

Mack, M., and Yanagita, M. (2015). Origin of myofibroblasts and cellular events triggering fibrosis. Kidney Int *87*, 297–307.

Manetti, M., Romano, E., Rosa, I., Guiducci, S., Bellando-Randone, S., De Paulis, A., Ibba-Manneschi, L., and Matucci-Cerinic, M. (2017). Endothelial-to-mesenchymal transition contributes to endothelial dysfunction and dermal fibrosis in systemic sclerosis. Ann. Rheum. Dis. *76*, 924–934.

Marangoni, R.G., Korman, B.D., Wei, J., Wood, T.A., Graham, L.V., Whitfield, M.L., Scherer, P.E., Tourtellotte, W.G., and Varga, J. (2015). Myofibroblasts in murine cutaneous fibrosis originate from adiponectin-positive intradermal progenitors. Arthritis Rheumatol *67*, 1062–1073.

Martini, E., Kunderfranco, P., Peano, C., Carullo, P., Cremonesi, M., Schorn, T., Carriero, R., Termanini, A., Colombo, F.S., Jachetti, E., et al. (2019). Single-cell sequencing of mouse heart immune infiltrate in pressure overload-driven heart failure reveals extent of immune activation. Circulation *140*, 2089–2107.

Martinod, K., Witsch, T., Erpenbeck, L., Savchenko, A., Hayashi, H., Cherpokova, D., Gallant, M., Mauler, M., Cifuni, S.M., and Wagner, D.D. (2017). Peptidylarginine deiminase 4 promotes age-related organ fibrosis. J. Exp. Med. *214*, 439–458.

Martins, V., Gonzalez De Los Santos, F., Wu, Z., Capelozzi, V., Phan, S.H., and Liu, T. (2015). FIZZ1-induced myofibroblast transdifferentiation from adipocytes and its potential role in dermal fibrosis and lipoatrophy. Am. J. Pathol. *185*, 2768–2776.

Mehta, H., Goulet, P.-O., Nguyen, V., Pérez, G., Koenig, M., Senécal, J.-L., and Sarfati, M. (2016). Topoisomerase I peptide-loaded dendritic cells induce autoantibody response as well as skin and lung fibrosis. Autoimmunity *49*, 503–513.

Metsalu, T., and Vilo, J. (2015). ClustVis: a web tool for visualizing clustering of multivariate data using principal component analysis and heatmap. Nucleic Acids Res. *43*, W566–W570.

Nagai, N., Ohguchi, H., Nakaki, R., Matsumura, Y., Kanki, Y., Sakai, J., Aburatani, H., and Minami, T. (2018). Downregulation of ERG and FLI1 expression in endothelial cells triggers endothelial-to-mesenchymal transition. PLoS Genet. *14*, 1–29.

Negmadjanov, U., Godic, Z., Rizvi, F., Emelyanova, L., Ross, G., Richards, J., Holmuhamedov, E.L., and Jahangir, A. (2015). TGF-β1-mediated differentiation of fibroblasts is associated with increased mitochondrial content and cellular respiration. PLoS ONE *10*, 1–12.

Onuora, S. (2015). Connective tissue diseases: adipocyte-myofibroblast transition: linking intradermal fat loss to skin fibrosis in SSc. Nat. Rev. Rheumatol. *11*, 63.

Phillips, J.E., Peng, R., Burns, L., Harris, P., Garrido, R., Tyagi, G., Fine, J.S., and Stevenson, C.S. (2012). Bleomycin induced lung fibrosis increases work of breathing in the mouse. Pulm. Pharmacol. Ther. *25*, 281–285.

Piera-Velazquez, S., and Jimenez, S.A. (2012). Molecular mechanisms of endothelial to mesenchymal cell transition (EndoMT) in experimentally induced fibrotic diseases. Fibrogenesis Tissue Repair *5*, S7.

R Core Team (2020). R: A Language and Environment for Statistical Computing (R Foundation for Statistical Computing).

Van Raemdonck, K., Gouwy, M., Lepers, S.A., Van Damme, J., and Struyf, S. (2014). CXCL4L1 and CXCL4 signaling in human lymphatic and microvascular endothelial cells and activated lymphocytes: Involvement of mitogen-activated protein (MAP) kinases, Src and p70S6 kinase. Angiogenesis *17*, 631–640.

Van Raemdonck, K., Van den Steen, P.E., Liekens, S., Van Damme, J., and Struyf, S. (2015). CXCR3 ligands in disease and therapy. Cytokine Growth Factor Rev. *26*, 311–327.

Rajkumar, V.S., Sundberg, C., Abraham, D.J., Rubin, K., and Black, C.M. (1999). Activation of microvascular pericytes in autoimmune Raynaud's phenomenon and systemic sclerosis. Arthritis Rheum. *42*, 930–941.

Rajkumar, V.S., Howell, K., Csiszar, K., Denton, C.P., Black, C.M., and Abraham, D.J. (2005). Shared expression of phenotypic markers in systemic sclerosis indicates a convergence of pericytes and fibroblasts to a myofibroblast lineage in fibrosis. Arthritis Res. Ther. *7*, R1113–R1123.

Raredon, M.S.B., Adams, T.S., Suhail, Y., Schupp, J.C., Poli, S., Neumark, N., Leiby, K.L., Greaney, A.M., Yuan, Y., Horien, C., et al. (2019). Single-cell connectomic analysis of adult mammalian lungs. Sci. Adv. *5*, 1–16.

Rice, L.M., Padilla, C.M., McLaughlin, S.R., Mathes, A., Ziemek, J., Goummih, S., Nakerakanti, S., York, M., Farina, G., Whitfield, M.L., et al. (2015). Fresolimumab treatment decreases biomarkers and improves clinical symptoms in systemic sclerosis patients. J. Clin. Invest. *125*, 2795–2807.

Rockey, D.C., Bell, P.D., and Hill, J.A. (2015). Fibrosis — a common pathway to organ injury and failure. N. Engl. J. Med. *372*, 1138–1149.

Sarabi, A., Kramp, B.K., Drechsler, M., Hackeng, T.M., Soehnlein, O., Weber, C., Koenen, R.R., and Von Hundelshausen, P. (2011). CXCL4L1 inhibits angiogenesis and induces undirected endothelial cell migration without affecting endothelial cell proliferation and monocyte recruitment. J. Thromb. Haemost. *9*, 209–219.

Schafer, S., Viswanathan, S., Widjaja, A.A., Lim, W.-W., Moreno-Moral, A., DeLaughter, D.M., Ng, B., Patone, G., Chow, K., Khin, E., et al. (2017). IL11 is a crucial determinant of cardiovascular fibrosis. Nature, 1–30.

Schaffner, A., Rhyn, P., Schoedon, G., and Schaer, D.J. (2005). Regulated expression of platelet factor 4 in human monocytes–role of PARs as a quantitatively important monocyte activation pathway. J. Leukoc. Biol. *78*, 202–209.

Scheuerer, B., Ernst, M., Dürrbaum-Landmann, I., Fleischer, J., Grage-Griebenow, E., Brandt, E., Flad, H.D., and Petersen, F. (2000). The CXC-chemokine platelet factor 4 promotes monocyte survival and induces monocyte differentiation into macrophages. Blood *95*, 1158–1166.

Schindelin, J., Arganda-Carreras, I., Frise, E., Kaynig, V., Longair, M., Pietzsch, T., Preibisch, S., Rueden, C., Saalfeld, S., Schmid, B., et al. (2012). Fiji: An open-source platform for biological-image analysis. Nat. Methods *9*, 676–682.

Schwarz, K.B., Rosensweig, J., Sharma, S., Jones, L., Durant, M., Potter, C., and Narkewicz, M.R. (2003). Plasma markers of platelet activation in cystic fibrosis liver and lung disease. J. Pediatr. Gastroenterol. Nutr. *37*, 187–191.

Silva-Cardoso, S.C., Affandi, A.J., Spel, L., Cossu, M., van Roon, J.A.G., Boes, M., and Radstake, T.R.D.J. (2017). CXCL4 exposure potentiates TLR-driven polarization of human monocyte-derived dendritic cells and increases stimulation of T cells. J. Immunol. *199*, 253–262.

Stifano, G., Affandi, A.J., Mathes, A.L., Rice, L.M., Nakerakanti, S., Nazari, B., Lee, J., Christmann, R.B., and Lafyatis, R. (2014). Chronic Toll-like receptor 4 stimulation in skin induces inflammation, macrophage activation, transforming growth factor beta signature gene expression, and fibrosis. Arthritis Res. Ther. *16*, R136.

Sundberg, C., Ivarsson, M., Gerdin, B., and Rubin, K. (1996). Pericytes as collagen-producing cells in excessive dermal scarring. Lab. Invest. *74*, 452–466.

Tamagawa-Mineoka, R., Katoh, N., Ueda, E., Masuda, K., and Kishimoto, S. (2008). Elevated platelet activation in patients with atopic dermatitis and psoriasis: increased plasma levels of beta-thromboglobulin and platelet factor 4. Allergol. Int. *57*, 391–396.

Trojanowska, M. (2010). Cellular and molecular aspects of vascular dysfunction in systemic sclerosis. Nat. Rev. Rheumatol. *6*, 453–460.

Tyndall, A.J., Bannert, B., Vonk, M., Airò, P., Cozzi, F., Carreira, P.E., Bancel, D.F., Allanore, Y., Müller-Ladner, U., Distler, O., et al. (2010). Causes and risk factors for death in systemic sclerosis: a study from the EULAR scleroderma trials and research (EUSTAR) database. Ann. Rheum. Dis. *69*, 1809–1815.

Valentini, G., Riccardi, A., Vettori, S., Irace, R., Iudici, M., Tolone, S., Docimo, L., Bocchino, M., Sanduzzi, A., and Cozzolino, D. (2017). CXCL4 in undifferentiated connective tissue disease at risk for systemic sclerosis (SSc) (previously referred to as very early SSc). Clin. Exp. Med. *17*, 411–414.

Valenzi, E., Bulik, M., Tabib, T., Morse, C., Sembrat, J., Trejo Bittar, H., Rojas, M., and Lafyatis, R. (2019). Single-cell analysis reveals fibroblast heterogeneity and myofibroblasts in systemic sclerosis-associated interstitial lung disease. Ann. Rheum. Dis. *78*, 1379–1387.

Vandercappellen, J., Noppen, S., Verbeke, H., Put, W., Conings, R., Gouwy, M., Schutyser, E., Proost, P., Sciot, R., Geboes, K., et al. (2007). Stimulation of angiostatic platelet factor-4 variant (CXCL4L1/PF-4var) versus inhibition of angiogenic granulocyte chemotactic protein-2 (CXCL6/GCP-2) in normal and tumoral mesenchymal cells. J. Leukoc. Biol. *82*, 1519–1530.

Vandercappellen, J., Van Damme, J., and Struyf, S. (2010). The role of the CXC chemokines platelet factor-4 (CXCL4/PF-4) and its variant (CXCL4L1/PF-4var) in inflammation, angiogenesis and cancer. Cytokine Growth Factor Rev. *4*, 1–18.

Varga, J., and Abraham, D. (2007). Systemic sclerosis: a prototypic multisystem fibrotic disorder. J. Clin. Invest. *117*, 557–567.

Volkmann, E.R., Tashkin, D.P., Roth, M.D., Clements, P.J., Khanna, D., Furst, D.E., Mayes, M., Charles, J., Tseng, C.-H., Elashoff, R.M., et al. (2016). Changes in plasma CXCL4 levels are associated with improvements in lung function in patients receiving immunosuppressive therapy for systemic sclerosis-related interstitial lung disease. Arthritis Res. Ther. *18*, 305.

Wickham, H., Averick, M., Bryan, J., Chang, W., McGowan, L., François, R., Grolemund, G., Hayes, A., Henry, L., Hester, J., et al. (2019). Welcome to the tidyverse. J. Open Source Softw. *4*, 1686.

Williamson, J.D., Sadofsky, L.R., and Hart, S.P. (2015). The pathogenesis of bleomycin-induced lung injury in animals and its applicability to human idiopathic pulmonary fibrosis. Exp. Lung Res. *41*, 57–73.

Xie, T., Wang, Y., Deng, N., Huang, G., Taghavifar, F., Geng, Y., Liu, N., Kulur, V., Yao, C., Chen, P., et al. (2018). Single-cell deconvolution of fibroblast heterogeneity in mouse pulmonary fibrosis. Cell Rep *22*, 3625–3640.

Xiong, J., Kawagishi, H., Yan, Y., Liu, J., Wells, Q.S., Edmunds, L.R., Fergusson, M.M., Yu, Z.-X., Rovira, I.I., Brittain, E.L., et al. (2018). A metabolic basis for endothelial-to-mesenchymal transition. Mol. Cell *69*, 689–698.e7.

Yeo, L., Adlard, N., Biehl, M., Juarez, M., Smallie, T., Snow, M., Buckley, C.D., Raza, K., Filer, A., and Scheel-Toellner, D. (2016). Expression of chemokines CXCL4 and CXCL7 by synovial macrophages defines an early stage of rheumatoid arthritis. Ann. Rheum. Dis. *75*, 763–771.

Zaldivar, M.M., Pauels, K., von Hundelshausen, P., Berres, M.-L., Schmitz, P., Bornemann, J., Kowalska, M.A., Gassler, N., Streetz, K.L., Weiskirchen, R., et al. (2010). CXC chemokine ligand 4 (Cxcl4) is a platelet-derived mediator of experimental liver fibrosis. Hepatology *51*, 1345–1353.

Zhang, W., Chen, G., Ren, J.-G., and Zhao, Y.-F. (2013). Bleomycin induces endothelial mesenchymal transition through activation of mTOR pathway: A possible mechanism contributing to the sclerotherapy of venous malformations. Br. J. Pharmacol. *170*, 1210–1220.

STAR★METHODS

KEY RESOURCES TABLE

REAGENT or RESOURCE	SOURCE	IDENTIFIER
Antibodies		
α-Smooth Muscle Actin (αSMA)	Sigma-Aldrich	Cat# A5228, RRID:AB_262054
Smooth muscle 22 α (SM22α)	Abcam	Cat# ab14106, RRID:AB_443021
α Tubulin	Sigma Aldrich	Cat# T6199, RRID:AB_477583
Vimentin	Cell Signal	Cat# 5741, RRID:AB_10695459
GAPDH	Life Technologies	Cat# MA5-15738, RRID:AB_10977387
Collagen-I	Southern Biotech	Cat# 1310-01, RRID:AB_2753206
Collagen-I	Millipore	Cat# AB745, RRID:AB_92134
Collagen-III	Millipore	Cat# AB747, RRID:AB_11211895
FLI1	BD Biosciences	Cat# 554266, RRID:AB_395333
β-actin	Abcam	Cat# ab8229, RRID:AB_306374
Phospho-Smad2 (Ser465/467)/ Smad3 (Ser423/425)	Cell Signaling	Cat# 8828, RRID:AB_2631089
CD45	BD Biosciences	Cat# 550539, RRID:AB_2174426
IRDye 680RD Donkey anti-rabbit IgG	Li-Cor	Cat# 925-68073, RRID:AB_2716687
IRDye 800CW Donkey anti-mouse IgG	Li-Cor	Cat# 925-32212, RRID:AB_2716622
HRP anti-goat IgG	SantaCruz	Cat# sc-2020, RRID:AB_631728
AlexaFluor 594 goat anti-rabbit IgG	Life Technologies	Cat# A-11037, RRID:AB_2534095
AlexaFluor 647 goat-anti-rabbit IgG	Life Technologies	Cat# A-21245, RRID:AB_2535813
Biological samples		
Mouse skin	This paper	N/A
Mouse heart	This paper	N/A
Mouse lung	This paper	N/A
Chemicals, peptides, and recombinant proteins		
Bleomycin (Bleomedac)	Medac GmbH	N/A
Recombinant human CXCL4 (PF4)	Peprotech	Cat# 300-16
RIPA buffer	Sigma	Cat# R0278
EGM-2 bullet kit	Lonza	Cat# CC-3162
Critical commercial assays		
RNeasy Mini Kit	Qiagen	Cat# 74106
iScript™ cDNA Synthesis Kit	Bio-Rad	Cat# 1708891
SYBR™ Select Master Mix	Thermo Fisher Scientific	Cat# 4472919
TaqMan™ Fast Advanced Master Mix	Thermo Fisher Scientific	Cat# 4444557
RT² Profiler PCR Arrays	Qiagen	Cat# 330231 PAMM-120ZA
RT² First Strand Kit	Qiagen	Cat# 330404
RT² SYBR Green ROX qPCR Mastermix	Qiagen	Cat# 330523
Total collagen assay QuickZyme	QuickZyme	Cat# QZBtotcol1
Deposited data		
Bleomycin-induced lung fibrosis	Xie et al. (2018)	GSE104154
Asbestos-induced lung fibrosis	Joshi et al., 2020	GSE127803
pressure overload-induced cardiac fibrosis	Martini et al. (2019)	GSE122930
SSc-associated interstitial lung disease	Valenzi et al. (2019)	GSE128169
Idiopathic pulmonary fibrosis	Habermann et al. (2020)	GSE135893

(*Continued on next page*)

Continued

REAGENT or RESOURCE	SOURCE	IDENTIFIER
Experimental models: Cell lines		
Human Dermal Fibroblasts	This paper	N/A
Human adipose stromal cells	This paper	N/A
Human Pulmonary Artery Endothelial Cells (HPAEC)	Thermo Fisher Scientific	Cat# C0085C
Human Umbilical Vein Endothelial Cells (HUVEC)	Thermo Fisher Scientific	Cat# C0155C
Human Brain Vascular Pericytes	ScienCell	Cat# 1200
Experimental models: Organisms/strains		
Mouse: C57BL/6	The Jackson Laboratory or internal breeding colonies of the University of Utrecht	000664
Mouse: *Cxcl4*−/−	Eslin et al. (2004)	http://www.informatics.jax.org/allele/key/34968
Mouse: hu*CXCL4*+	Eslin et al. (2004)	N/A
Mouse: BALB/c	Janvier	SC-BALBJ
Mouse: B10.D2	The Jackson Laboratory	000461
Oligonucleotides		
Oligonucleotide primers are listed in Table S3		
Software and algorithms		
FlowJo v10	FlowJo	https://www.flowjo.com/solutions/flowjo, RRID:SCR_008520
ImageJ/Fiji v1.8, v2.1	Schindelin et al., 2012	https://fiji.sc, RRID:SCR_002285
ClustVis	Metsalu and Vilo (2015)	https://biit.cs.ut.ee/clustvis/, RRID:SCR_017133
R v4.0.4	R Core Team, 2020	http://www.r-project.org/, RRID:SCR_001905
RStudio v1.3.1093	RStudio	https://rstudio.com/, RRID:SCR_000432
Seurat v3.2.3	Butler et al. (2018)	https://satijalab.org/seurat/get_started.html, RRID:SCR_016341
Connectome v0.2.2	Raredon et al. (2019)	https://msraredon.github.io/Connectome/
Tidyverse	Wickham et al. (2019)	https://www.tidyverse.org/, RRID:SCR_019186
Scripts and computational analysis	This study	https://github.com/MolecularCellBiologyImmunology/CXCL4_fibrosis
GraphPad Prism 8.1.2	GraphPad	https://www.graphpad.com, RRID:SCR_002798

RESOURCE AVAILABILITY

Lead contact

Further information and requests for resources and reagents should be directed to and will be fulfilled by the lead contact, Wioleta Marut (vmarut@gmail.com).

Materials availability

This study did not generate new unique reagents.

Data and code availability

This paper analyzes existing, publicly available data. These accession numbers for the datasets are listed in the key resources table. R scripts used in this study are available on github (https://github.com/MolecularCellBiologyImmunology/CXCL4_fibrosis). Any additional information required to reanalyze the data reported in this paper is available from the lead contact upon request.

EXPERIMENTAL MODEL AND SUBJECT DETAILS

Cell culture

Normal human dermal fibroblasts were isolated as described before (Kabala et al., 2017) and cultured in DMEM medium (Thermo Fisher Scientific) supplemented with 10% fetal bovine serum (FBS, Biowest) and 1% penicillin-streptamycin (pen/strep). For adipose stromal cells, fat was removed from the dermis and epidermis and cut into small pieces. The epidermis was removed from the dermis after dispase incubation. Both dermis and adipose tissue were incubated in collagenase type II (Gibco, Invitrogen, Paisly, UK)/dispase II (Roche, Mannheim, Germany) solution for 2 h at 37°C, passed through a 40 μm cell strainer, and cultured (Kroeze et al., 2009). Human pulmonary arterial endothelial cells (HPAEC) and human umbilical vein endothelial cells (HUVEC, both from Thermo Fisher Scientific) were cultured in EBM-2 media supplemented with EGM-2 bullet kit (both Lonza) and 10% FBS, in 0.2% bovine skin gelatin-coated (Sigma Aldrich) culture vessels. Human brain pericytes (Sciencell) were cultured in DMEM medium supplemented with 10% FBS, 1% pen/strep in 0.1% gelatin-coated (Costar) culture plates. Cells were cultured at 37°C in humidified atmosphere containing 5% CO_2. Fibroblasts, endothelial cells, and pericytes were prestarved prior to stimulation with recombinant human CXCL4 (Peprotech) in basal media with low serum for 24 - 48 h.

Animal experiments

Animal experiments were approved by the Committee on Animal Experiments of the University of Utrecht and by the institutional animal care and used committee at Boston University Medical Campus. Experiments were performed at the Central Animal Laboratory, Utrecht University, The Netherlands or Boston University School of Medicine. Cxcl4−/− and huCXCL4+ mice were generated in the Children's Hospital of Philadelphia and were backcrossed onto the C57BL/6 background as described before (Eslin et al., 2004). Cxcl4−/− mice were generated by replacing the entire coding region for mouse Cxcl4 (also known as Pf4; 1.16 kb) with a 1.8-kb *neo* gene. huCXCL4+ mice are transgenic with a 10-kb fragment of the human PF4 locus with 5.4 kb of upstream and 3.8 kb of downstream sequence. All mice used in this study were matched for age and sex as described below, kept under specific pathogen-free conditions, and food and water were provided ad libitum.

Bleomycin-induced skin and lung fibrosis

Bleomycin-induced SSc was developed using daily subcutaneous injections of bleomycin (200 μL, 500 μg/mL, Bleomedac, Medac) into the back of adult female mice (either WT, Cxcl4−/− or huCXCL4+ on C57BL/6 background) for the duration of two to four weeks (n = 12 per group or n = 6 per group per each time point). Mice were at least 12 weeks of age, with average body weight of 27 g (WT, 25.7 ± 5.2 g; Cxcl4−/−, 26.9 ± 3.5 g; huCXCL4+, 27.8 ± 3.6 g) and none of the mice showed excessive weight loss (20% of the initial body weight). When indicated, mice were treated for 10 days with 200 μg of rabbit anti-murine CXCL4 (Bethyl Laboratories, Montgomery, TX, USA) delivered subcutaneously every other day. Two days after the last treatment, mice were treated with 200 μL, 0.15 mg/kg, of buprenorphine (Temgesic), anesthetized with 5% isoflurane for blood collection, and sacrificed by cervical dislocation. Serum was collected after centrifugation at 1700 xg for 10 min. Skin biopsies were obtained from the back region using biopsy punch (4 mm diameter). Tissues were stored in medium for cell culture, homogenized in RLT buffer for RNA isolation, frozen in RIPA buffer for immunoblotting, or snap frozen for collagen quantification. For histology, cannula was inserted into trachea and fixed with ligature, and lungs were instilled with 4% formalin. Skin biopsies were placed in between two foam pads in a histology cassette and fixed with 4% formalin. Following formalin fixation, tissues were embedded in paraffin and cut into 5 μm sections for further analysis. Dermal fibroblasts were extracted from minced skin biopsies after digestion with 2.5 mg/mL collagenase from Clostridium histolyticum (Sigma Aldrich) at 37°C for 2 h with agitation. Debris were removed by 70 μm cell strainer and cells were washed in medium. Cells were cultured in DMEM/F-12 supplemented with 10% FBS at 37°C until near confluency.

In vivo administration of TLR ligands

Mini osmotic pumps (Alzet), were implanted to adult mice (C57BL/6, 6-8 weeks) (n = 3-4) under anesthesia as described previously (Stifano et al., 2014). Osmotic pumps were designed to deliver 1 μL of PBS or stimuli per h over 7 days in a total of 200 μL volume. 500 μg/mL of poly(I:C) or lipopolysaccharide (LPS-EB ultrapure, both Invivogen) were used. After 7 days, mice were sacrificed and the skin (∼1 cm^2) surrounding or distal to the pump outlet was homogenized in TRIzol (Invitrogen) for total RNA preparation.

Induction of Scl-GvHD in mice

Scl-GvHD was induced following splenocyte and bone marrow transplantation from male B10.D2 (H-2d; Jackson Laboratory) to female BALB/c mice (Janvier Laboratory) as described previously (Kavian et al., 2012). Briefly, recipient mice were lethally irradiated with 750cGy from a Gammacel (137Cs) source. After 3 h, they were injected intravenously with donor spleen cells ($2x10^6$ per mouse) and bone marrow cells ($1x10^6$ per mouse) that were previously removed of red blood cells using ammonium chloride solution and suspended in RPMI-1640 (Gibco). The control group received syngeneic BALB/c spleen and bone marrow cells. We used 9 mice per group. Mice were sacrificed by cervical dislocation after four weeks and blood was collected for serum preparation.

Transverse aortic constriction

WT or Cxcl4−/− mice were subjected to transverse aortic constriction (TAC) or sham surgery as previously described (de Haan et al., 2017). Briefly, mice were anaesthetized, intubated, and connected to a respirator with a 1:1 oxygen-air ratio. A core body temperature of 37°C was maintained during surgery by an experienced surgeon. Using a minimally-invasive approach, the aortic arch was reached between two ribs after midline incision in the anterior neck. Transverse aortic constriction was placed between the brachiocephalic artery and the left common artery against a blunt 27-gauge needle with a 7–0 silk suture followed by prompt removal of the needle. Sham operated mice underwent the same procedure without aortic constriction. Correct placement of the TAC was confirmed after 7 days by measuring the flow in the aortic arch and in the carotid arteries (flow ratio between left and right carotid ≥ 5 were included). After the indicated time points, mice were euthanized using sodium pentobarbital, blood was collected for serum measurement of cytokines, hearts were perfused with saline and fixed in formalin for histological analysis, or snap frozen for RNA isolation. Mice phenotypic characteristics and echocardiographic measurements are listed in Tables S1 and S2.

METHOD DETAILS

RNA isolation and quantitative PCR

Total RNA was isolated from cell lysates using the RNeasy MiniPrep Kit (Qiagen), followed by retrotranscription with iScript reverse transcriptase kit (Biorad), or superscript IV (Life Technologies) according to the manufacturer's instructions. Expression of protein-coding genes was analysed by real-time quantitative-PCR (qPCR) using SybrSelect mastermix with 300-500 nM primer pairs, or Taqman reactions on a StepOne Plus or QuantStudio 12k flex (Thermo Fisher Scientific). qPCR data were normalized to the expression of GUSB (human) or Rpl13 and B2m (mouse) housekeeping genes. The mouse fibrosis PCR array (Qiagen) was used according to manufacturer's instructions and normalized to Gapdh and Hsp90 using QuantStudio software. Heatmap was generated using ClustVis software (http://biit.cs.ut.ee/clustvis/) (Metsalu and Vilo, 2015) clustered using correlation distance with complete linkage, or GraphPad Prism. Primers used are listed in Table S3.

Western blotting

Cells were lysed in RIPA buffer (Sigma Aldrich) with Complete Protease inhibitor (Roche). Protein content was determined by BCA assay (Pierce) and samples were denatured in Laemmli buffer (Bio-Rad) at 95°C for 10 min 5-10 μg of protein was loaded to Mini-PROTEAN TGX 4-20% gels (Bio-Rad), separated by electrophoresis, and blotted with a nitrocellulose Trans-blot Turbo transfer pack, according to manufacturer's instructions (all from Bio-Rad). After blocking for 1 h in 5% (m/v) milk, blots were incubated with primary antibody at 4°C overnight, followed with secondary antibody for 1 h at room temperature (RT), and washed in Tris-buffered saline with 0.2% Tween-20 in between steps. Protein bands were developed using ECL (GE Healthcare) and measured on Molecular Imager GelDoc (Bio-Rad) or were detected using infrared fluorescence detection on Odyssey imager (Li-Cor). Antibodies used are listed in Table S4.

Extracellular matrix deposition assay

1,500 human dermal fibroblasts were seeded and cultured on 384-well black imaging plate (Greiner) in Fibroblast Basal Medium supplemented with Fibroblast Growth Kit, Low serum (2% (v/v) FBS, ATCC) at 37°C for one week with medium replenishment every two days. Presto Blue was used to monitor cell viability (Thermo Fisher Scientific). Recombinant human CXCL4 was added as indicated. After decellularization, matrices were fixed with 100% ice-cold methanol at −20°C for 30 min, blocked with 1% (v/v) normal goat serum in phosphate-buffered saline (PBS) for 30 min at RT, incubated with primary antibody in PBS for 1.5 h at RT, followed by secondary antibody in PBS for 1 h at RT, with PBS washes in between steps. Matrices were imaged at the Pathway 855 bio-imaging system (BD Biosciences) using the AttoVision software, and quantified with ImageJ software.

Collagen gel contraction assay

Collagen I was isolated from rat tails and reconstituted in 0.1% acetic acid (4 mg/mL). Fibroblasts and ASCs were seeded in 4 mg/mL collagen I solution at $2x10^5$ cells/ml and 1 mL gel/well was poured into 12 wells plates. Gels were allowed to polymerize for 2 h at 37°C. Gels were detached from the well surface to allow contraction and normal culture medium was added to the wells. Medium (including CXCL4) was replaced 3 times per week. Pictures were taken using a Canon Powershot G12 camera and gel surface was measured using ImageJ software.

Endothelial tubule formation assay

Collagen-based 3D co-cultures was described previously (Chrifi et al., 2017) and performed as the following: lenti-GFP-transduced human umbilical vein endothelial cells (HUVECs) and lenti-dsRED-transduced human brain vascular pericytes were suspended in endothelial basal medium (Lonza) at a respective 5:1 ratio in collagen type I (2.0 mg/mL). Using NaOH, pH was set to 7.5, after which the cells were seeded in flat-bottomed 96 well plates followed by 1 h incubation at 37°C to enable collagen solidification. Next, 100 μL medium was added after which the co-cultures were incubated at 37°C for another 24 h. Subsequently, medium containing CXCL4 was added to final concentrations of 0, 2, and 4 μg/mL CXCL4. After 72 h of culture, fluorescently labeled co-cultures were imaged and analyzed using Angiosys software.

Metabolic assays

OCRs were measured in HPAEC activated for 24 h using XF media (non-buffered RPMI 1640 containing 10 mM glucose, 2 mM L-glutamine, and 1 mM sodium pyruvate) under basal conditions and in response to 1μM oligomycin, 5μM FCCP, and 1μM rotenone on XF-96 Extracellular Flux Analyzers (Seahorse Bioscience). Maximal respiration was the OCR difference between uncoupler FCCP and rotenone.

Immunofluorescence of mouse fibroblasts *ex vivo*

Mouse fibroblasts were seeded at equal number on clear bottom 96-wells black imaging plate (Ibidi) and rested overnight. Cells were fixed with 50 μL 4% paraformaldehyde, and blocked and permeabilized with 5% (v/v) normal donkey serum, 5% (v/v) normal goat serum, 0.3% (v/v) Triton X-100, in PBS for 1 h at RT. Cells were incubated with anti-αSMA (Sigma Aldrich) in antibody diluent (PBS with 10% [v/v] bovine serum albumin (BSA) and 0.3% (v/v) Triton X-100) for overnight at 4°C, followed by incubation with secondary antibody in antibody diluent for 1 h at RT, with PBS washes in between steps. Cell nuclei were visualized by Hoechst staining. Fibroblasts were imaged at the Pathway 855 bioimaging system (BD Biosciences) using AttoVision software, and quantified with ImageJ software.

Tissue immunohistochemistry and immunofluorescence

Formalin-fixed, paraffin-embedded skin and heart sections or 4% PFA-fixed, 0.25% Triton X 100-permeabilized cells were stained with appropriate primary antibodies, including rabbit anti-αSMA for 1 h (Abcam), goat anti-collagen I for 1 h, (Southern biotech), mouse anti-PDGFR-β for overnight (Santa Cruz), rabbit anti-pSMAD2/3 for overnight (Cell Signaling), and rabbit anti-CD31 for overnight (Abcam). Counter staining of cell nuclei was performed using DAPI (Santa Cruz Biotechnology). Both tissue sections and cultured cells and were incubated with isotype control antibodies (Santa Cruz Biotechnology). Stained sections and cells were visualized using a bright field or fluorescence microscope (BH2 and BX41 Olympus). For quantification, integrated density was analyzed using ImageJ Software.

Measurement of secreted proteins

The level of CXCL4 in mouse sera was measured by enzyme-linked immunosorbent assay (R&D). Levels of soluble KC, E-selectin, and L-selectin, were measured by multiplex immunoassay (Millipore) based on xMAP technology (Luminex) at the MultiPlex Core Facility of the Center for Translational Immunology, University Medical Center Utrecht (de Jager et al., 2005). For the Luminex-based assay, acquisition was performed with a Bio-Rad FlexMap3D system using Xponent 4.2 software and analyzed using Bio-Plex Manager 6.1.1.

Histochemical analysis

Consecutive 5-μm skin, lung, and heart sections of paraffin-embedded tissue were stained with Masson's trichrome, to evaluate collagen content and organization. Dermal thickness was determined at five different locations per slide for each mouse by two blinded, experienced researchers using ImageJ. Color deconvolution plugin was used to quantify collagen staining (Chen et al., 2017).

Quantification of tissue collagen

Collagen content was quantified by colorimetric assays from 4 mm skin punch biopsies. Skin sections were transferred into a microcentrifuge tube and upon addition of 150 μL 6 M HCl hydrolyzed by overnight incubation at 95°C in a heat block, and collagen content was determined in supernatants by QuickZyme total collagen assay (QuickZyme Bioscience).

Single-cell RNA sequencing analysis

We used published datasets of single-cell RNA sequencing from mouse bleomycin-induced lung fibrosis (GSE104154) (Xie et al., 2018), asbestos-induced lung fibrosis (GSE127803) (Joshi et al., 2020), and pressure overload-induced cardiac fibrosis by TAC (GSE122930) (Martini et al., 2019), patients with SSc-associated interstitial lung disease (GSE128169) (Valenzi et al., 2019), and patients with pulmonary fibrosis (GSE135893) (Habermann et al., 2020). Data was analyzed using Seurat R toolkit (version 3.2.3) (Butler et al., 2018; R Core Team, 2020; Wickham et al., 2019). Connectome ligand-receptor analysis was performed using Connectome (version 0.2.2) (Raredon et al., 2019), using literature-supported ligands and cell surface receptors curated in the FANTOM5 database.

QUANTIFICATION AND STATISTICAL ANALYSIS

Mann Whitney's test or one-way ANOVA corrected for multiple comparison by controlling false discovery rate (FDR) were calculated using GraphPad Prism Software as appropriate. Differences of (adjusted) *$p < 0.05$, **$p < 0.01$, ***$p < 0.001$, ****$p < 0.0001$, were considered significantly different and they were reported in the figures and figure legends. N represents biological or independent replicates, bars represent mean ± SD unless indicated otherwise.